Universal relations for neutron star math xmlns="http://www.w3.org/1998/Math/MathML" display="inline">mi>f/mi>/math>-mode and math xmlns="http://www.w3.org/1998/Math/MathML" display="inline">mi>g/mi>/math>-mode oscillations

Tianqi Zhao and James M. Lattimer

Phys. Rev. D **106**, 123002 — Published 2 December 2022

DOI: 10.1103/PhysRevD.106.123002

Universal Relations for Neutron Star f-mode and g-mode Oscillations

Tianqi Zhao[1, 2, *] and James M. Lattimer[2]

[1] *Department of Physics and Astronomy, Ohio University, Athens, OH 45701, USA*
[2] *Dept. of Physics & Astronomy, Stony Brook University, Stony Brook, NY 11794-3800*

(Dated: November 15, 2022)

Among the various oscillation modes of neutron stars, f- and g- modes are the most likely to be ultimately observed in binary neutron star mergers due to their relatively large coupling and shared frequencies with tidal excitations. The f-mode frequency and damping time are known to correlate in normal neutron stars with their compactness, and previous fits to hadronic stars are extended and shown to be valid for an extremely broad sampling of equations of state using a piecewise polytropic parameterization scheme for hadrons and a constant sound-speed parameterization for quark matter. Separate fits applicable to quark (self-bound) stars are improved. Much more significant correlations exist with tidal deformability, and therefore with moment of inertia and quadrupole moment. It is conclusively demonstrated that these correlations are the same for all types of stars, whether hadronic, hybrid, or pure quark, and its accuracy is quantified. A novel 1-node branch of the f-mode that occurs in low-mass hybrid stars in a narrow mass range just beyond the critical mass necessary for a phase transition to appear is identified. This 1-node branch shows the largest, but still small, deviations from the universal correlation for any configuration. It is characterized by a non-monotonic relation between neutron star mass and f-mode frequency, in contrast to the behavior otherwise observed in normal, quark and hybrid stars.

The g-mode only exists in matter with a non-barotropic equation of state involving temperature, chemical potential or composition (such as being out of beta equilibrium), or a phase transition in barotropic matter. The g-mode therefore could serve as a probe for studying phase transitions in hybrid stars. In contrast with the f-mode, g-mode frequencies do not correlate well with tidal deformability, but depend strongly on properties of the transition (the density and the magnitude of the discontinuity) at the transition. Imposing causality and maximum mass constraints, a fit involving neutron star and phase transition properties is found and the g-mode frequency is determined to have an upper bound of about 1.25 kHz. However, if the sound speed c_s in the inner core at densities above the phase transition density is restricted to $c_s^2 \leq 1/3$, g-mode frequencies can only reach about 0.8 kHz, which are significantly lower than f-mode frequencies (1.3-2.8 kHz). g-mode gravitational wave damping times are found to be extremely long, $> 10^4$ s (10^2 s) in the inner core with $c_s^2 \leq 1/3$ (1), in comparison with f-mode damping times (0.1-1 s).

I. INTRODUCTION

Isolated neutron stars (NSs) are expected to oscillate in many modes, corresponding to different restoring forces. In asteroseismology, fluid oscillations, including g-, f- and p-modes, have been extensively studied in Newtonian gravity [1]. In this paper, we focus on f- and g-modes under linearized general relativity formalism [2, 3]. The f-mode is the lowest-order, fundamental, non-radial breathing mode, characterized by a zero radial node number $n = 0$. The g-mode is a global oscillation with an arbitrary number of nodes with gravity being the dominant restoring force. They are a consequence of local buoyancy oscillations, and characterized by small Eulerian pressure variations. The f- and g-modes we consider have $\ell = 2$ so that they may couple with gravitational waves.

In addition, one could consider also p- and w-modes that have an arbitrary number of nodes. The restoring force of the p-mode is dominated by pressure variations in matter. The w-mode is the strongly damped gravitational wave (GW) mode dominated by variations of the space-time metric [4]. However, p- and w-modes are excited only marginally during neutron star mergers due to their high frequencies, 5-12 kHz [5]. In any case, such high frequencies are effectively unobservable, being well beyond the range of next-generation GW detectors. We will not consider them further.

The f-mode is a fundamental mode sitting between the g- and p-modes, with frequency $\nu_f = \omega_f/(2\pi) \sim 1.3-2.8$ kHz. The frequency of f-mode is known to correlate with the mean NS density $\omega_f \propto \sqrt{G\bar{\rho}} \propto \sqrt{M/R^3}$ [6]. However, a more precise, EOS-insensitive, correlation can be found between the dimensionless frequency $\Omega_f = GM\omega_f/c^3$ with other NS properties such as the dimensionless moment of inertia $\bar{I} = Ic^4/(G^2M^3)$ and the dimensionless tidal deformability Λ. A semi-universal $\Omega_f - \bar{I}$ correlation was first proposed by Lau et. al. [7], established with a limited number of EOSs. Later, the so-called I-Love-Q relation was discovered [8] that provides a rather precise, EOS-insensitive, correlation between $\bar{I}$, Λ, and the dimensionless quadrupole moment. Thus, there exists a similar $\Omega_f - \Lambda$ correlation as well [9–11]. In this work, we refine this correlation to encompass any causal EOS constrained by neutron star mass observations and low-density neutron matter studies employing a polytropic parameterization scheme to model matter at

* zhaot@ohio.edu

supra-nuclear densities. We have explored a much wider variety of EOSs than in previous works. In addition, we quantify the accuracy and bounds of this correlation and show that it also applies to self-bound (pure quark) and hybrid (hadron-quark) stars with strong phase transitions.

There are normally three types of non-zero frequency g-modes corresponding to instabilities when matter moves adiabatically through temperature, chemical composition or density discontinuity. The local g-mode frequency ν_g is determined by the Brunt-Vaisala frequency,

$$\nu_g^2 = g^2 \left(\frac{1}{c_e^2} - \frac{1}{c_s^2} \right) e^{\nu - \lambda}, \tag{1}$$

where ν and λ are the temporal and radial metric functions. Here, $g = (dp/dr)(\varepsilon + p)^{-1}$ is the local gravity, p and ε are the pressure and energy density, respectively, $c_e = \sqrt{dp/d\varepsilon}$ is the equilibrium sound speed and $c_s = \sqrt{\gamma p (\mu n_B)^{-1}}$ is the adiabatic sound speed , both in units of c. $\gamma = (n_B/p)\partial p/\partial n_B$ is the adiabatic index defining how the matter reacts to the adiabatic compression. $\mu = \partial\varepsilon/\partial n_B$ and n_B are the chemical potential and baryon number density, respectively. g-mode buoyancy oscillations are stable when $\nu_g^2 > 0$, while $\nu_g^2 < 0$ corresponds to a convective region. When matter is marginally buoyant, the g-mode has zero frequency. When the thermal [12] or chemical [13, 14] relaxation time scale is longer than the oscillation period, the sound speed in temperature and chemical equilibrium is different from that of the moving, perturbed, matter. For the thermal and chemical g-modes, an arbitrary number of nodes exist, and the principle g-modes with n=1 have the highest frequency. A universal relation between chemical g-mode frequency and lepton fraction was discovered recently [15] providing key information about the symmetry energy at high density. However, these frequencies are relatively small ($\lesssim 0.6$ kHz) in most cases, except for exotic matter involving quarks and hyperons [15, 16]. A g-mode due to a density discontinuity from a phase transition can be understand as a special version of a g-mode due to chemical composition changes, since matter on the low-density side can be treated as having a different composition from that on the high-density side. This situation occurs when matter does not instantaneously change phase upon passing through the phase transition boundary. For this reason, this type of g-mode is also known as an i-mode (interface mode) in the literature [17, 18]. Higher order g-modes do not exist, unless there are multiple density discontinuities. Both the frequency and damping times of an i-mode are significantly larger than that of other g-modes and are more likely to be observed in gravitation wave observations [18]. When there is more than one phase transition (density discontinuity) in a NS, multiple groups of g-modes could exist [19]. We will focus on the particular type of g-mode, which we will call the discontinuous g-mode, with lowest order $n = 1$.

Quadruple oscillations ($\ell = 2$) of all modes can couple to and lead to emission of GW radiation, and will be characterized by the GW damping timescale τ. It is of interest to estimate the observability of this radiation. The amplitude of observed oscillations with frequency ω is [20]

$$h(t) = h_0 e^{-t/\tau} \cos \omega t, \tag{2}$$

where $h_0 = h(0)$. The observed GW energy flux is

$$F(t) = \frac{c^3 \omega^2 h_0^2}{16\pi G} e^{-2t/\tau} \tag{3}$$

$$= 3.17 e^{-2t/\tau} \left(\frac{\nu}{\rm kHz} \right)^2 \left(\frac{h_0}{10^{-22}} \right)^2 \ {\rm ergs\ cm^{-2}\ s^{-1}}, \tag{4}$$

The total GW energy is $E = 4\pi D^2 \int_0^\infty F dt$, where the source distance is D, or

$$E = \frac{c^3 \omega^2 h_0^2 \tau D^2}{8G} \tag{5}$$

$$= 4.27 \times 10^{49} \left(\frac{\nu}{\rm kHz} \right)^2 \left(\frac{h_0}{10^{-23}} \right)^2 \left(\frac{\tau}{0.1\ {\rm s}} \right) \left(\frac{D}{15\ {\rm Mpc}} \right)^2 {\rm ergs}. \tag{6}$$

The total radiated energy in corresponding oscillations should be larger than this energy, since bulk viscosity also contributes to dissipation. We use this formula as a lower limit for the radiated energy in this oscillation mode in order to be conservative. To scale this relation, we use a typical frequency $\nu = 1$ kHz, damping time $\tau = 0.1$ s, and distance $D = 15$ Mpc (the distance to the Virgo Cluster). The Advanced LIGO noise power spectrum (sensitivity) at that frequency is about $S_n = 4 \times 10^{-24}$. Thus, to be potentially observable in Advanced LIGO with a signal-to-noise ratio ~ 2.5 would require $h_0 \sim 10^{-23}$ and a total radiated GW energy $E \sim 4 \times 10^{49}$ ergs. With a next-generation instrument such as Cosmic Explorer and Einstein Telescope that has about 10 times the sensitivity of Advanced LIGO, the threshold values become $h_0 \sim 10^{-24}$ and $E \sim 4 \times 10^{47}$ erg.

There are multiple scenarios for pumping energy into NS oscillations, including core-collapse supernovae, NS mergers, close encounters of a NS with a black hole (BH), and NS starquakes [5]. The requisite energy can be compared with the results of hydrodynamic simulations, which offer powerful methods to study oscillations of proto-NSs from core-collapse supernovae and of rapidly rotating supramassive NSs from NS mergers [21]. Core-collapse supernovae have long been considered as promising GW sources [22]. f- and g-mode oscillations can be identified in recent simulations and show the total GW energy in core-collapse supernovae of order $10^{44} - 10^{47}$ ergs depending on the mass and rotation rate of the progenitor [23]. Thus, only galactic sources with $D < 20$ kpc are likely to be observed in Advanced LIGO observations, at a rate of, at best, a few per century [24]. Next-generation instruments such as Cosmic Explore improves the distance threshold to $D < 200$ kpc, but won't change the observed rate much since additional large galaxies lie outside this distance. Since a proto-NS is hot and opaque to neutrinos, its mean density is smaller and their f-mode frequencies should be smaller than that of a cold NS.

For comparison, rapidly rotating supramassive NS remnants from NS mergers have masses likely larger than $M_{\rm max}$, the maximum mass of cold, non-rotating NS, being temporarily supported by rotation acquired from the binary's orbital angular momentum [25]. Due to their large expected ellipticities and oscillation amplitudes, a GW energy from $10^{-2}M_\odot c^2$ to $10^{-3}M_\odot c^2$ could be emitted within 5 ms [26]. In this case, the observable distance range for an advanced LIGO signal-to-noise ratio of 2.5 is estimated to be $D \lesssim 20-45$ Mpc for Advanced LIGO observations [27, 28]. The binary neutron star merger rate has been estimated to be 320^{+490}_{-240} Gpc^{-3} yr^{-1} based on the O1 and O2 LIGO–Virgo observation runs as well as on the first half of the O3 run [29]. Thus, the predicted event rate becomes more favorable, ranging from 6×10^{-4} yr^{-1} to 0.04 yr^{-1}. With next-generation instruments such as Cosmic Explorer [30], the predicted event rate improves further to 0.06 yr^{-1} to 4 yr^{-1}, which now becomes reasonable.

Gravitational radiation observed in the post-merger phase is complicated by spin-oscillation interactions. Neutron star merger simulations show that the dominant fluid oscillation of a supramassive NS coincides with the $m = 2$ f-mode [31], and has a strong correlation with the isolated NS f-mode frequency [11], especially for equal-mass mergers. In the case of equal-mass mergers, the peak frequency in supramassive NSs is almost equal to that of the non-rotating f-mode frequency of isolated NSs with the same mass as each of the merging components [32].

Besides directly observing gravitational waves from post-merger NS oscillations, there might be additional indirect observational possibilities during the inspiral phase. During the inspiral, quadruple oscillations could be excited by the periodic tidal interaction from a companion, especially when the orbital frequency approaches the oscillation frequency [33]. Orbital energy transferred to quadruple oscillation results in dissipation and an extra phase advance in the gravitational waveform, and could have a large effect [34]. Because the g-mode has a low frequency, tidal interactions could excite g-mode oscillations well before resonances with the f-mode are reached during the last part of the inspiral.

Since the f-mode frequency is much higher than the orbital frequency, resonant excitations of the f-mode are not likely for non-rotating NSs. However, if an inspiralling NS is counter-rotating, f-mode resonant frequencies could be lowered significantly because the relevant frequency is $\omega_f - 2\omega_s$, where ω_s is the spin frequency. The f-mode has a larger coupling with tidal field compared with the g-mode. For a millisecond pulsar, f-mode resonances in this case could cause phase advances up to hundreds of cycles [34, 35]. However, large phase shifts due to a resonance seemed not to have occurred in the case of the recent binary NS merger GW170817, since its waveform is consistent with a low spin prior. In any case, binary evolution theory favors low spins as well [36], rendering this scenario as unlikely.

Interestingly, a crude estimate of f-mode frequencies of neutron stars can be obtained by combining observations with the information described above. Dynamical tidal effects can be modeled based on an effective-one-body approach, treating tidal deformability and f-mode frequency as key parameters [37–39]. A lower bound to the f-mode frequency can be estimated from the non-detection of a significant resonance phase shift, while an upper bound can be estimated from the $\Omega_f - \Lambda$ universal relation previously alluded to. The resulting 90% credible interval of f-mode frequency for GW170817 was reported as 1.43 kHz $< \nu_f <$ 2.90 kHz for the more massive star and 1.48 kHz $< \nu_f <$ 3.18 kHz [40] for the less massive star.

Another source of NS oscillations could be starquakes that lead to the release of the strain energy in the neutron star crust. Starquakes might have a connection with glitches observed in pulsar timing. Glitch models based on superfluid vortex models generally predict a negligible amount of GW radiation [41]. But glitch models involving starquakes could transfer large amount of rotational energy to f-mode oscillations [42]. Based on thousands of observed pulsar glitches, frequency changes range from 10^{-10} Hz to 10^{-4} Hz [43]. Assuming a solid rotation as assumed in starquake models, the change of rotational energies therefore range from 10^{34} ergs to 10^{43} ergs [44]. Therefore, only an event very close to the Earth $D \lesssim 3$ pc - 100 kpc) could be observable even in next-generation instruments. The closest known pulsar, RX J1856-3754, is about 0.12 kpc away, which lies within the observable range. Assuming a uniform pulsar distribution implies the existence of about 10^6 pulsars within the Galaxy. However, only about 3000 pulsars are observed [45], giving an average distance of about 1.3 kpc to the nearest pulsar, and indicating that most remain undetected. Based on decades of pulsar monitoring, about 10% of observed pulsars show glitches [46]. If a similar percentage of unobserved pulsars are capable of glitching, at most a few might lie in the observed range of next-generation instruments.

In this paper, we calculate f-mode and g-mode frequencies and damping times by solving relativistic non-radial oscillation equations [3, 47] which form an ordinary differential equation (ODE) eigenvalue problem. The f-mode is the mode with zero radial nodes in these calculations, and the g-mode is the mode with a single radial node having the next-lower frequency than the f-mode. In such calculations, NSs are usually assumed to be non-rotating, although rotation could slightly increase the f-mode frequency [48]. Going beyond the slow-rotation limit requires a more complicated solution involving the time evolution with partial differential equations [49], which could be calculated from dynamical non-linear GR simulation [50, 51]. Previous studies have mainly focused on hadronic NS. The few existing calculations involving quark stars and hybrid NSs generally have assumed an MIT bag model with $c_s^2 \approx 1/3$ for the NS inner core [52–54]. However, we will study models incorporating

higher sound speeds in both bare quark stars and in the inner core of hybrid NSs. We employ a parameterized hadronic EOS omitting temperature and chemical composition dependence, as discussed in Section III, allowing us to explore a wide variety of hadronic, hybrid and pure quark NSs. Since our parameterized EOS doesn't have temperature and chemical composition information, we study NS oscillations in equilibrium (i.e., equal equilibrium and adiabatic sound speeds) for both hadronic and hybrid configurations. A long transition timescale is assumed at quark-hadron interfaces, meaning that particle concentrations are frozen during oscillations at the interface.

Many previous studies, especially for hybrid NSs and quark stars, have used the Cowling approximation [53–58], which lacks dissipation due to gravitational waves. The Cowling approximation introduces about a 20-30% error in the f-mode frequency [10, 59, 60], which is significantly less accurate than that of the $\Omega_f - \bar{I} - \Lambda$ universal relation to be studied [7, 9, 10]. An 5% error in the g-mode frequency [60] from the Cowling approximation has also been found in $M \leq 1.2M_\odot$. Massive NSs with stronger gravity, in principle, result in even larger error in g-mode from the Cowling approximation [15]. Although non-linear numerical simulations reproduce the f-mode frequency, their damping times depart from linear perturbation theory [50]. Instead, we solve metric perturbation equations together with fluid perturbation equations to study the oscillation mode frequencies and gravitational damping time scales, see Appendix A for details. In Sec. II we illustrate this formalism applied in the case of Newtonian geometry to selected analytic equations of state, and compare to general relativistic results with and without Cowling approximation. In Sec. III we develop a six-parameter hadronic EOS together with a two-parameter extension to describe a hybrid EOS. Results for the f-mode are presented in Sec. V, where the EOS-insensitive $\Omega_f - \bar{I} - \Lambda$ relation is constructed. We determine bounds for these relations and quantify their uncertainties. Other fitting formulae are also described. We describe, for the first time, a special 1-node branch of the f-mode associated with so-called twin stars whose masses are near the transition mass to hybrid stars in Sec. VI. The discontinuous g-mode, present in stars with a phase transition density discontinuity, is analyzed in Sec. VII, where an EOS-insensitive correlation with stellar compactness is developed and quantified.

II. NEWTONIAN F-MODE FREQUENCY WITH ANALYTICAL EOSS

Much insight can be gained by comparing general relativistic results for realistic EOSs with simplified cases involving analytical EOSs both in general relativity and Newtonian gravity. Despite the fact that relativistic corrections are substantial, Newtonian analyses are valuable to justify the nature of the overall scaling of relativistic universal relations, and, in fact, can be more reliable than calculations using the relativistic Cowling approximation. In Newtonian physics, a variational analysis on the hydrostatic equilibrium equations with a linear solenoidal velocity perturbation leads to the Kelvin-mode frequency [61]

$$\omega^2_{Kelvin} = G\frac{2\ell(\ell-1)}{2\ell+1}\frac{\int_0^R \varepsilon(r) r^{2\ell-3} m(r) dr}{\int_0^R \varepsilon(r) r^{2\ell} dr} = G\frac{2\ell(\ell-1)(2\ell-1)}{2\ell+1}\frac{\int_0^R p(r) r^{2\ell-2} dr}{\int_0^R \varepsilon(r) r^{2\ell} dr} \quad (7)$$

where ℓ is the angular quantum number. The second equality in the above uses the hydrostatic equilibrium equations. The Kelvin-mode frequency can be a good approximation to the f-mode frequency of low-mass NSs with realistic EOSs [9], which we confirm below for $M \lesssim 1.4M_\odot$ or $\beta \lesssim 0.14$, where $\beta = GM/(c^2R)$ is the compactness. According to Eq. (7), Newtonian Kelvin-mode frequencies for the analytic EOSs must satisfy $\omega^2_{Kelvin} = CGM/R^3$ [6], or $\Omega^2_{Kelvin} = C\beta^3$, where the coefficients C are displayed in Table I. Fig. 1 compares those values to numerical general relativistic results. A slightly weaker dependence on β is apparent for the relativistic results for more massive and compact, but still observable, stars. Because the damping time originates from the general relativistic calculation, and is not defined in the Newtonian calculation, there is no simple analytic estimate for its β-dependence.

TABLE I. Newtonian coefficients $C = \Omega^2_{Kelvin}/\beta^3$ for analytic EOSs

EOS	$\ell = 2$	$\ell = 3$	$\ell = 4$
Inc	4/5	12/7	8/3
T VII	4/3	204/77	152/39
Buch	$3\pi^2(5\pi^2-30)^{-1}$	2.94766	4.24121

In the case of an homogeneous incompressible sphere (Inc), the energy density is constant, $\varepsilon(r) = \varepsilon_*$, and one finds [62]

$$C = \frac{2\ell(\ell-1)}{2\ell+1}. \quad (8)$$

This EOS will be seen to be a good approximation to that of pure quark stars.

In the case of the Tolman VII [63] (T VII) solution, the energy density has a quadratic dependence, $\epsilon(r) = \varepsilon_c[1-(r/R)^2]$, and

$$C = \frac{2\ell(\ell-1)(2\ell+11)}{(2\ell+1)(2\ell+5)}. \quad (9)$$

This analytic solution is seen to be an excellent approximation to the realistic SLy4 EOS for observable neutron stars in the relativistic case for both f-mode frequencies and damping times.

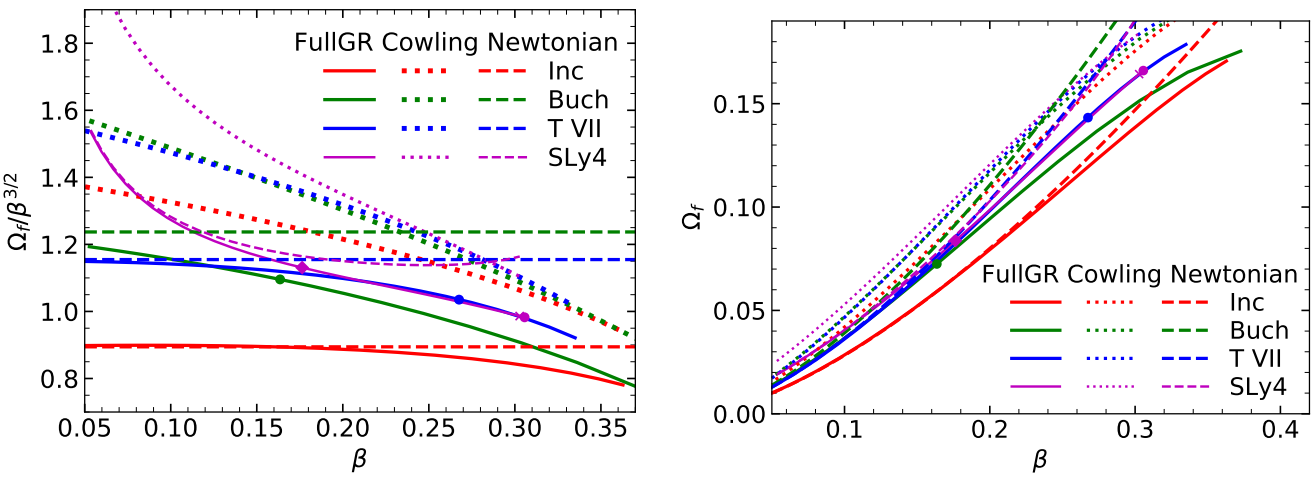

FIG. 1. Dimensionless f-mode frequency versus compactness β for the SLy4 and three analytic EOSs. Solid lines show the result of linear perturbation theory in general relativity, dashed lines show the Newtonian result (i.e., the Kelvin-mode frequency), and dotted lines show results assuming the Cowling approximation. Dots on the SLy4, T VII and Buch solid lines indicate β values where causality $c_s = 1$ occurs; the diamond on the SLy4 solid lines indicates the $1.4M_\odot$ configuration.

A third analytical solution is due to Buchdahl [64] (Buch), and it is the only one stemming from an analytic EOS, $\varepsilon = 12\sqrt{p_* p} - 5p$ where p_* is a constant. In the Newtonian limit, Buch becomes equivalent to the $n = 1$ polytropic EOS $p = \varepsilon^2/(144 p_*)$, for which $\varepsilon(r) \propto (R/r)\sin(r/R)$ and

$$C = -\frac{2\ell(\ell-1)\ {}_1F_2(\ell - \frac{1}{2}; \frac{3}{2}, \ell + \frac{1}{2}; -\pi^2)}{(2\ell - 3)\ {}_1F_2(\ell + \frac{1}{2}; \frac{3}{2}, \ell + \frac{3}{2}; -\frac{\pi^2}{4})}, \qquad (10)$$

where ${}_AF_B$ is the generalized hypergeometric function. This analytic solution has less success approximating a realistic EOS such as SLy4 than does T VII.

The relativistic Cowling approximation is applied to the three analytic and the SLy4 EOS, see dotted lines in Fig. 1, and is seen to generally overestimate Ω_f by 20-30%. In case of Inc, the deviations exceed 40% at low compactness where the Newtonian result is extremely accurate. Even in the SLy4 case, the Newtonian estimation is much more reliable except for extreme compactness where the error introduced by static Newtonian gravity dominates over that due to ignoring gravitational perturbations.

III. EOS FOR HADRONIC, HYBRID AND PURE QUARK STARS

We are interested in hadronic, pure quark and hybrid NSs with first-order phase transition. Previous studies of NS f-and g-modes with first-order phase transitions used polytropic EOSs with the same polytropic index for both low- and high-density parts of EOS [60, 65] or various hadronic EOSs with the MIT bag model [52–54]. An improvement we seek is to calculate with a more general hadronic NS EOS constrained by χEFT N3LO calculations [66] and causality coupled, if necessary, to constant sound speed matter at densities above a first-order phase transition.

The well-understood outer crust EOS is dominated by relativistic degenerate electron with pressure $p_e = (3/\pi^2)^{1/3} n_e^{4/3}/4$ with a small (negative) contribution from the ionic lattice. Dripped neutrons appear in the NS inner crust and slightly further modify the pressure. The hadronic contributions cause no more than a 10% deviation from p_e. Uncertainties in the nuclear interaction in the crust have a relatively negligible effect compared with uncertainties in the core EOS. As a result we use the same fixed crust EOS for all hadronic and hybrid NSs in this study. We employ an analytic crust EOS nearly identical to Table II in [67] to describe matter in the range $n_B < n_0 = 0.04$ fm^{-3} to avoid interpolation errors and to speed up the eigenvalue solver so that a multitude of models may be considered. Our choice of $n_0 = 0.04$ fm^{-3} is lower than the SLy4 core-crust interface density where the pressure could vary over 10% with different core EOS models [68]. As a result, the complete SLy4 crust, which extends to higher density, is not used as our fixed crust EOS. This procedure necessitates small parameter changes but allows for exploration of a wider range of high-density EOSs.

Read et al. [67] found the pressure–density relation of many proposed high-density EOS models could be relatively faithfully rendered using three polytropic segments, each segment being described by $p = K_i n^{\gamma_i}$ within the region $n_{i-1} < n < n_i$ where $i \in [1-3]$. Continuity of both pressure p and energy density ε at the core-crust transition density and polytropic segment boundaries determine K_i, leaving 6 free parameters, n_i and γ_i. Equivalently, n_i and p_i can be used as parameters. Within the

polytropic segment i, the energy density is given by

$$\varepsilon = \varepsilon_{i-1}\frac{n}{n_{i-1}} + \frac{p - p_{i-1}(n/n_{i-1})}{\gamma_i - 1}, \quad n_{i-1} \le n \le n_i. \tag{11}$$

The polytropic exponents and the energy densities at the boundaries are given by

$$\begin{aligned} \varepsilon_i &= \frac{p_i}{\gamma_i - 1} + \left(\varepsilon_{i-1} - \frac{p_{i-1}}{\gamma_i - 1}\right)\frac{n_i}{n_{i-1}}, \\ \gamma_i &= \ln(p_i/p_{i-1})/\ln(n_i/n_{i-1}). \end{aligned} \tag{12}$$

We take $n_0 = 0.04$ fm^{-3}, $\varepsilon_0 = 37.88$ MeV fm^{-3}, $p_0 = 0.1239$ MeV fm^{-3} from the crust EOS of SLy4. Following Read et al., we choose $n_1 = 0.3$ fm^{-3}, $n_2 = 0.6$ fm^{-3}, $n_3 = 1.2$ fm^{-3} [67]. The polytrope for $n_0 < n < n_1$ is fitted to $\pm\sigma$ ($\pm 2\sigma$) NS matter EOS with a χEFT N3LO calculation [66], giving $p_1 = 15.63 \pm 3.54$ (± 7.09) MeV fm^{-3}. The EOS in the higher density region $n > n_1$ is controlled by p_2 and p_3, which are free parameters limited by causality and maximum neutron star mass constraints [69]. The bounds for p_2 and p_3, as functions of p_1, can be found in Figs. 2 and 3 in Ref. [70]. We generate about 3000 hadronic EOSs by exploring the entire allowed ranges of p_1, p_2 and p_3. This 3-parameter model is called *PP3*.

For the high-density matter above the phase transition in hybrid stars, or for strange quark stars, we use a constant sound speed parameterization (called *CSS*) [71]. In high-density matter with $p > p_t$ in hybrid stars, one has

$$\varepsilon = (p - p_t)/c_s^2 + \varepsilon_t + \Delta\varepsilon \tag{13}$$

where p_t is the pressure at the first-order phase transition, ε_t is the energy density at the low-density side of the phase transition, $\Delta\varepsilon$ is the density jump at ε_t, and c_s is the (constant) sound speed for $p > p_t$.

There are 3 parameters for the *CSS* part of the hybrid EOS; $n_t/n_s \in [1, 4]$, $\Delta\varepsilon/\varepsilon_t \in [0.1, 1]$, and $c_s^2 \in [1/3, 1]$. In order to minimize parameters in the hadronic EOS for hybrid stars, we only vary p_1 within the 2σ χEFT band and fix $p_2 = 7.3p_1$ and $p_3 = 7.3p_2$, so that $\gamma_2 = \gamma_3 = 2.868$ for $n > n_1$ whenever needed. We therefore utilize only 3 hadronic EOSs, which we call N3LO-cen and N3LO$\pm\sigma$, for hybrid stars. Note that this is not the same as using the published N3LO EOS, which is only given up to about $2n_s$, but employs a particular extrapolation for $n > 2n_s$ as described in Ref. [66]. In total, there are 4 parameters for the hybrid stars.

In pure quark stars at all densities

$$\varepsilon = p/c_s^2 + \varepsilon_{surf} \tag{14}$$

where ε_{surf} is the energy density at the surface (where $p = 0$). The quark and hybrid expressions are the same when $p_t = \Delta\varepsilon = 0$ and $\varepsilon_t = \varepsilon_{surf}$. For the pure quark EOS, there are only two parameters, c_s and ε_{surf}.

IV. F-MODE FREQUENCIES OF HADRONIC, HYBRID AND QUARK STARS

We first compare f-mode frequencies as a function of stellar mass for pure quark stars (i.e., self-bound stars) using the *CSS* parameterization with those for representative hadronic EOSs corresponding to the central values of the neutron matter calculation (N3LO-cen) and its one-sigma uncertainty bounds (N3LO$\pm\sigma$) for all densities in excess of the crust-core boundary , see Fig. 2. In this example, quark stars have a c_s^2 range from 1/3 to 1 while the other parameter, ε_{surf}, is selected to give a maximum neutron star mass $M_{\rm max}$ from 2.0 to 2.6 $M_\odot$. Note that quark stars with smaller $M_{\rm max}$ have larger f-mode frequencies, and that in all cases, the frequency increases with stellar mass. Quark stars also have a lower limiting frequency whereas the hadronic frequencies decrease continuously with decreasing mass. Damping times for quark stars, on the other hand, generally decrease with mass except near $M_{\rm max}$ and there is no threshold damping time.

Next we explore the behavior of hybrid stars in Fig. 3. Various values of n_t, $\Delta\varepsilon/\varepsilon_t$ and c_s^2 are utilized. No restrictions are placed on $M_{\rm max}$ for this study. The hadronic EOS N3LO-cen is used for the hadronic parts of the hybrid stars. For $n_t = n_s$, the phase transition occurs for masses so small that the resulting f-mode frequencies and damping times show a similar behavior to those of pure quark stars. Just above the transition masses, the frequencies increase more rapidly with mass for hybrid stars than for the N3LO-cen hadronic stars, but this behavior can reverse close to $M_{\rm max}$. Note that large f-mode frequencies are not possible for low-mass hadronic and hybrid NSs, which provides a possible observable to distinguish the existence of a quark star. In this example, a $1.M_\odot$ ($1.5M_\odot$) NS with f-mode frequency larger than 2.1 kHz (2.4 kHz) must be a quark star unless 2-σ PNM bounds are violated.

Next, we proceed to an examination comparing larger numbers of hadronic, hybrid and quark matter stars in order to identify systematic trends. Fig. 4 shows the relation between the f-mode frequency and the stellar compactness for thousands of stars of varying mass: hadronic stars having a fixed crust with the *PP3* parameterized EOS, hybrid stars having a four-parameter EOS with a fixed crust, and the three parameter *CSS* quark matter stars, all subject to the constraints of causality and $M_{\rm max} \ge 2M_\odot$. As expected from our earlier comparison of SLy4 and the three analtyic EOSs, there is a global correlation between Ω_f and β. However, in contrast to the Newtonian studies, the purely linear relation between Ω_f and $\beta^{3/2}$ is broken. The right-hand panel in Fig. 4 shows that the effective power of β that would best fit quark stars remains close to 3/2, but best fits to the body of hadronic and hybrid stars is considerably less than 3/2.

We find a power-law fit with the minimum uncertainty, applicable to hadronic and hybrid stars with $M \ge 1M_\odot$,

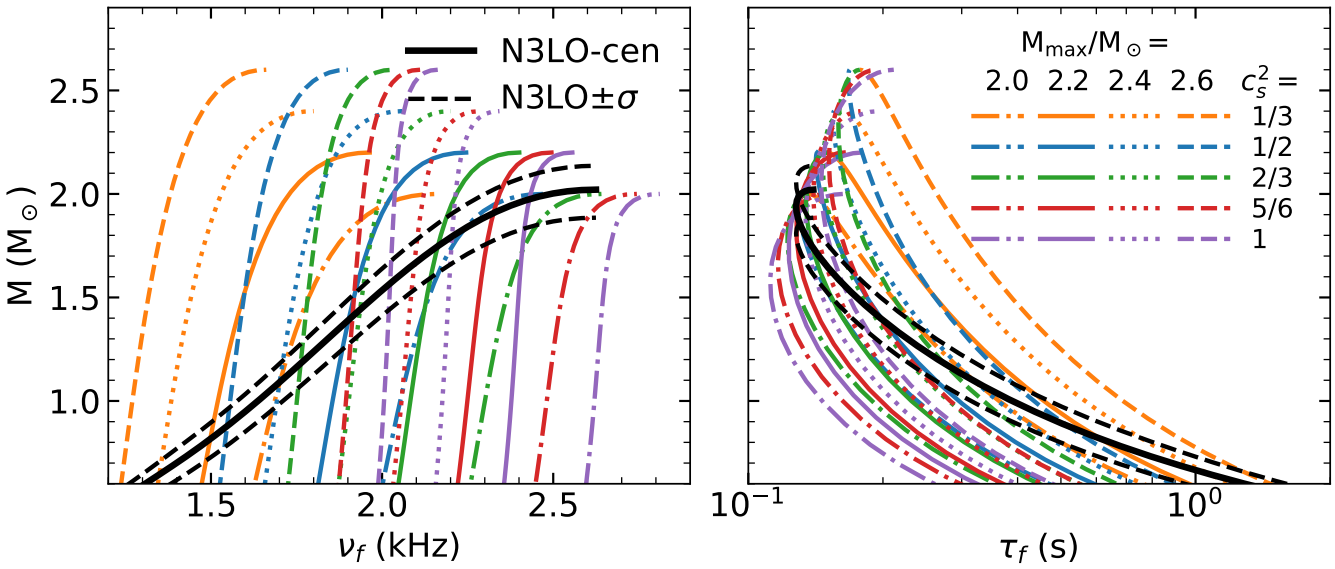

FIG. 2. The left (right) panel shows the f-mode frequency (damping time) as a function of M for pure quark stars with the CSS parameterization (colored curves) compared to hadronic stars employing the N3LO-cen EOS and its one-sigma uncertainty bounds (black curves).

is

$$\Omega_f = A\beta^{5/4}, \tag{15}$$

where $A = 0.714 \pm 0.056$ for hadronic stars and $A = 0.711 \pm 0.072$ for hybrid stars (see the left panel of Fig. 5). This is clearly shown by the much smaller dynamic range of the vertical axis in this figure compared to the right-hand panel of Fig. 4. In contrast, pure quark stars follow the Newtonian trend of $\beta^{3/2}$. If we further impose the GW170817 binary tidal deformability constraint $\tilde{\Lambda}_{GW170817} < 521$ [72], the respective values of A stay the same for hadronic stars and $A = 0.720 \pm 0.063$ for hybrid stars (see the right panel of Fig. 5). This figure demonstrates how well a measure of Ω_f is able to place a tight constraint on β.

In summary, we have found a simple power-law fit relating Ω_f to $\beta^{5/4}$ for all hadronic and hybrid stars that has only an 8% uncertainty.

Previously, a general power expansion of $\Omega_f(\beta)$ has shown to also be relatively accurate [11, 74]. With our parametric approach, we refine the accuracy of such relations for hadronic, hybrid and quark NSs and extend the study to damping times in Fig. 6. We fit the hadronic and hybrid $\Omega_f - \beta$ results for $M \geq 0.7M_\odot$ with

$$[\Omega_{f-\beta}]_H = \sum_{i=0}^{2} a_i\beta^i + \left(\sum_{i=4}^{6} a_i\beta^i\right)\mathbf{i} \tag{16}$$

The lower panels in Fig. 6 show the maximum deviation of this fit for all sampled configurations of each type. The average deviations are much smaller. This relation fits Re[Ω_f] for hadronic stars slightly better than for hybrid NSs, and to better than 6.3% (11.5%) accuracy for all physically-relevant configurations. Damping times are fit to a similar precision 13.5% for hadronic stars, but the maximum uncertainty for hybrid stars is about 23.8%. It is seen that the Buch and T VII solutions are good representations for both hadronic and hybrid stars. The $\Omega_f - \beta$ relation for frequencies and damping times for pure quark stars are much closer to the Inc analytic case, due to lack of a soft compressible crust. For the pure quark case, we employ the fit

$$[\Omega_{f-\beta}]_Q = a_0\beta^{3/2} + \left(\sum_{i=4}^{6} a_i\beta^i\right)\mathbf{i} \tag{17}$$

applicable to stars with $M \geq 1M_\odot$ using results for $M \geq 0.7M_\odot$. The precision of the quark $\Omega_f - \beta$ relation is about 7.6% for the real part and 6.1% for the imaginary part. The Inc analytic model is a good representation of quark stars.

The bottom panels in Fig. 6 also show the maximum deviations for hadronic stars developed by Refs. [74] (Tsui), [6] (Andersson), and [11, 75] (Lioutas). For the f-mode frequency, Tsui and Lioutas fitted results from 9 (20) hadronic EOSs from $0.12 < \beta < 0.28$ to a quadratic formula. We checked that adding an additional term doesn't offer much improvement, but by altering parameters we were able to improve the fit at large compactnesses. For the f-mode damping time, Tsui also used a quadratic formula, but Andersson used expressions with fourth and fifth power terms using results from 12 hadronic EOSs in the range $0.15 < \beta < 0.28$. Lioutas improved this fit by adding a sixth power term. We checked that adding additional terms offers no further improvement. Overall, our fit for the f-mode frequency for hadronic stars is not a substantial improve-

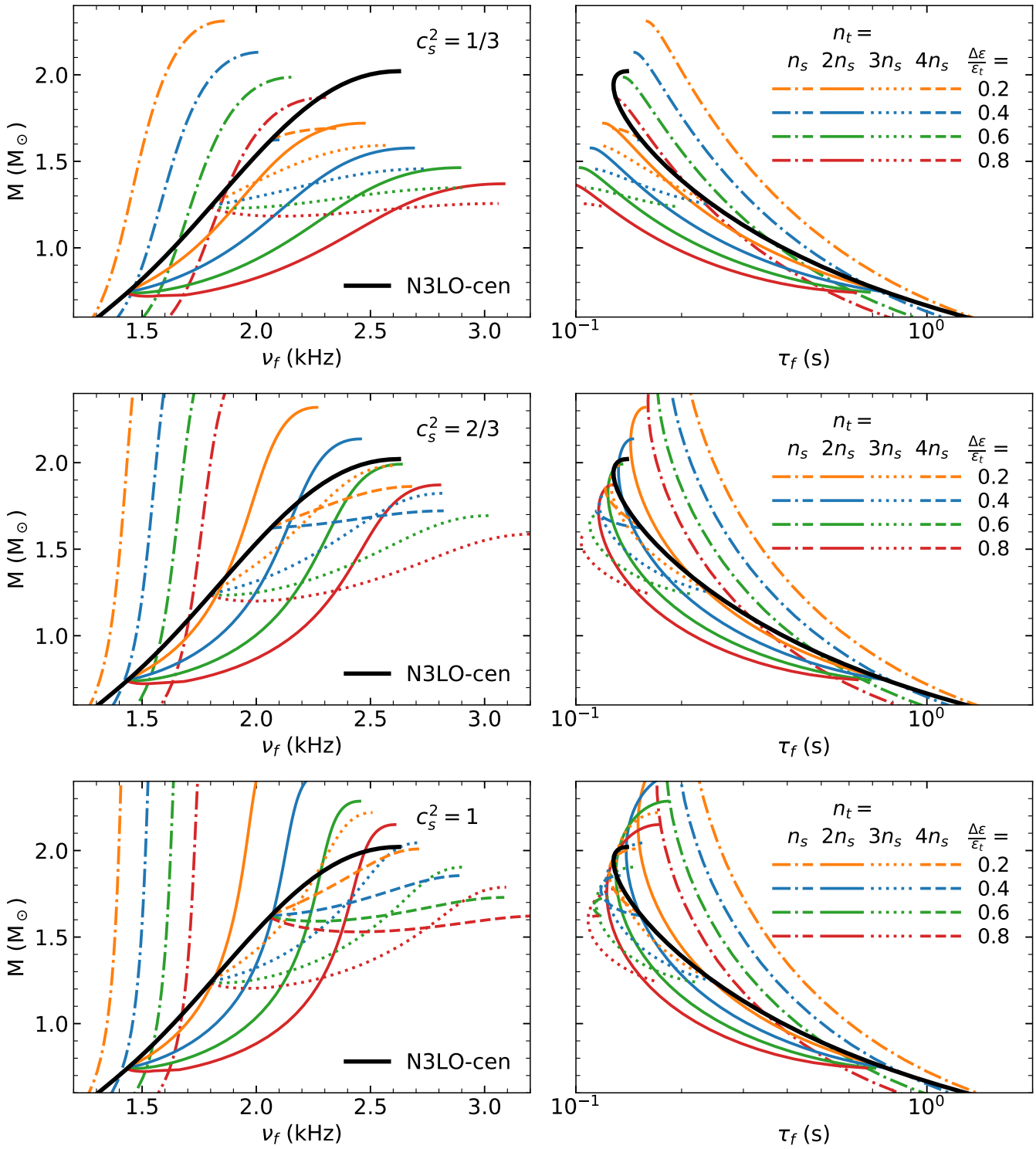

FIG. 3. The same as Fig. 2 but for hybrid NSs with the hadronic EOS fitted to N3LO-cen and *CSS* sound speeds $c_s^2 = [1/3, 2/3, 1]$ from top to bottom, respectively.

ment over previous fits except for $\beta \gtrsim 0.25$, but we have now established the validity of these fits for a much more complete sampling of physically possible hadronic EOSs, and further established their validity for hybrid configurations which had heretofore not been tested. Our fit for the damping time for hadronic EOSs is a substantial improvement over previous fits, and we have further established its validity for hybrid stars. Furthermore, we

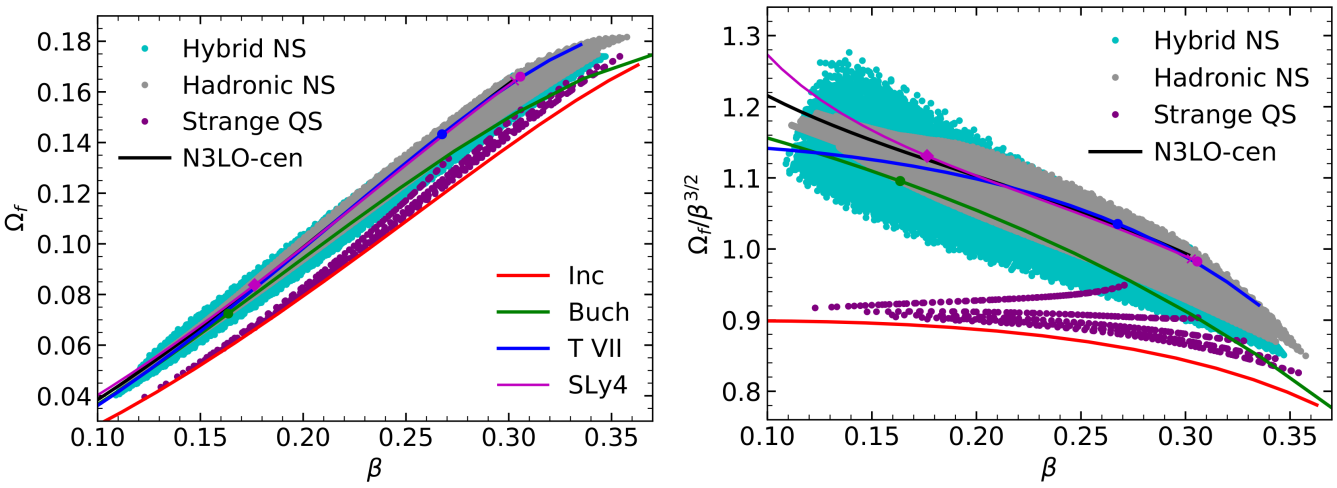

FIG. 4. The dimensionless f-mode frequency Ω_f as a function of stellar compactness β for parameterized hadronic, hybrid and quark matter stars constained by causality and $M_{\rm max} \geq 2M_\odot$. General relativistic results for the analytic EOSs and the SLy4 and N3LO-cen hadronic EOSs are shown for comparison.

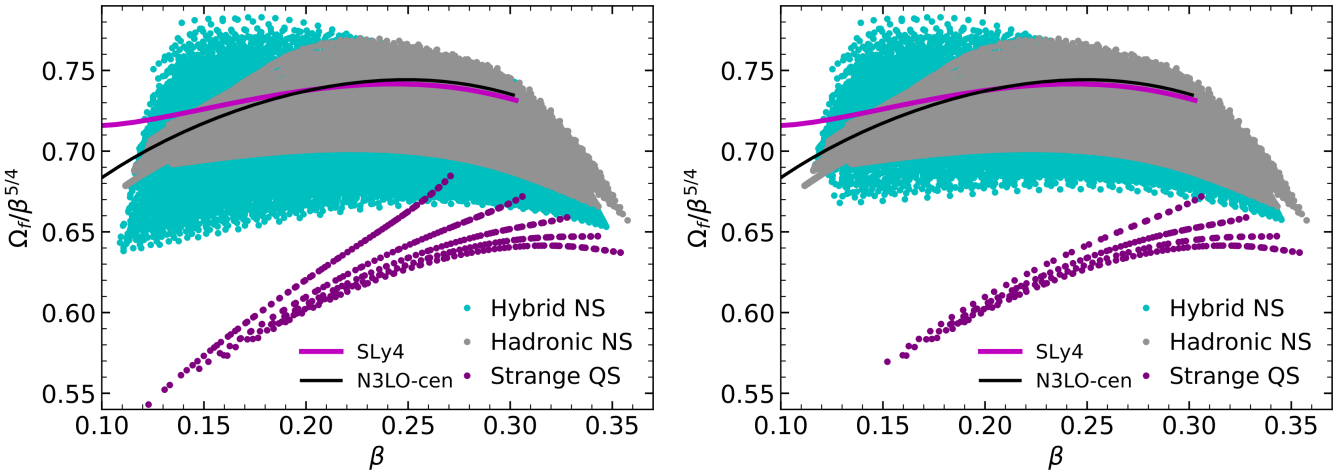

FIG. 5. Left: the same as the right panel of Fig. 4 but with the y-axis replaced by $\Omega_f\beta^{5/4}$. Right: the same as the left panel but including the additional GW170817 $\tilde{\Lambda}$ constraint [72].

find that previous fits are poor fits to f-mode frequencies and damping times for quark stars, and we established accurate fits for these cases.

V. $\Omega_f - \bar{I} - \Lambda$ RELATIONS

A much more precise EOS-insensitive relation relates Ω_f to $\bar{I}$, as first shown by Lau et. al. [7]. However, Ref. [7] only used a small sample of 11 EOSs. Later, the EOS-insensitive $\bar{I} - \Lambda - Q$ relation was discovered [8], suggesting a similarly good $\Omega_f - \Lambda$ relation should also exist , which was confirmed by Refs. [9–11], but also using limited samples of EOSs. The relations regarding the f-mode are much tighter than similar relations involving other modes, e.g. p-modes [6], and w-modes [73]. However, Ref. [77] claimed quark matter EOSs violate the hadronic $\Omega_f - \bar{I} - \Lambda$ relation.

We extended previous results by testing the accuracy of the $\Omega_f - \bar{I} - \Lambda$ relation for extremely large samples of hadronic, quark and hybrid NS. We established fits valid for all three stellar categories, hadronic, hybrid and quark, for $M \geq 1.0M_\odot$ using results for $M \geq 0.7M_\odot$:

$$\Omega_{f-\bar{I}} = \sum_{i=0}^{6} a_i \bar{I}^{-i/2} \tag{18}$$

$$\Omega_{f-\Lambda} = \sum_{i=0}^{6} a_i (\ln \Lambda)^i \tag{19}$$

Figs. 7 and 8 show the $\Omega_f - \bar{I} - \Lambda$ relations for hadronic, hybrid and quark NS. Fitting parameters are given in

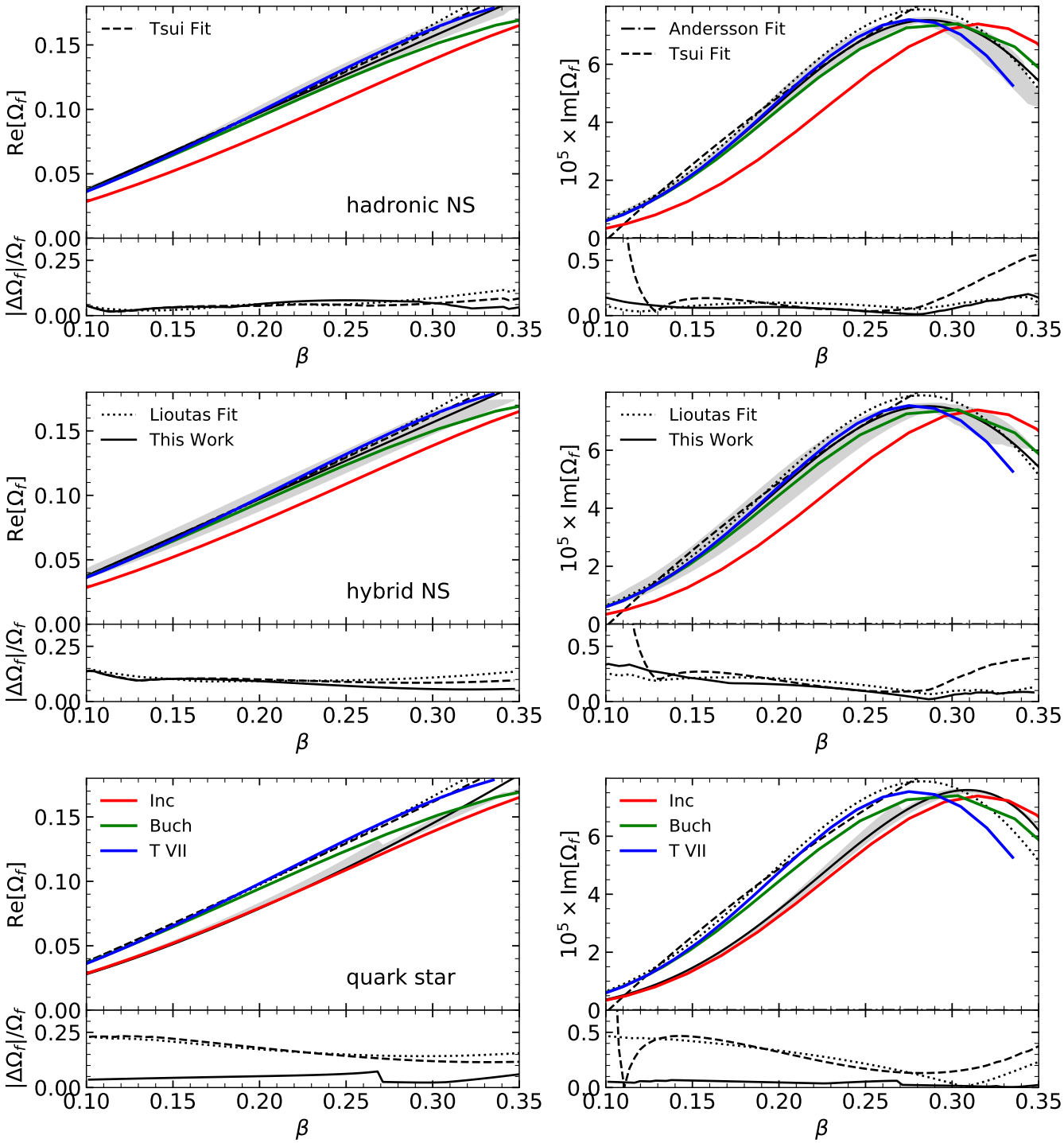

FIG. 6. The $\Omega_f - \beta$ EOS insensitive relations. The left (right) panel shows the real (imaginary) part of the dimensionless frequency. The top, middle, and the bottom panels are for hadronic, hybrid, pure quark (self-bound) EOSs, respectively. Grey regions represent results with different EOSs for hadronic NS, hybrid NS and quark star. "This Work" refers to the fits of Eq. (16) for hadronic and hybrid stars and Eq. 17 for pure quark stars. Fits due to Refs. [74] (Tsui), [6] (Andersson), and [11, 75] (Lioutas) are also shown. The lower parts of each panel show maximum deviations of each fit from the full computed results for all configurations studied in this work.

h

TABLE II. Fitting parameters of real and imaginary parts of Ω_f in Eqs. (16) - (19).

	a_0	a_1	a_2	a_3	a_4	a_5	a_6	a_7
$[\Omega_{f-\beta}]_H$	-0.02223	0.5982	-0.007331	0	0.1048	-0.4971	0.5943	0
$[\Omega_{f-\beta}]_Q$	0.8811	0	0	0	0.05352	-0.1849	0.1253	0
$\mathrm{Re}[\Omega_{f-\bar{I}}]$	0.09006	-2.41	29.47	-179.8	659.5	-1427	1689	-845.4
$\mathrm{Im}[\Omega_{f-\bar{I}}]$	7.506e-05	-0.002054	0.02363	-0.1484	0.5589	-1.226	1.493	-0.8139
$\mathrm{Re}[\Omega_{f-\Lambda}]$	0.1817	-0.006652	-0.004105	0.0004072	1.712e-05	-4.796e-06	2.838e-07	-5.743e-09
$\mathrm{Im}[\Omega_{f-\Lambda}]$	4.514e-05	1.907e-05	4.3e-06	-5.025e-06	1.133e-06	-1.165e-07	5.851e-09	-1.167e-10

Table II. No star of any category with $M > 1M_\odot$ significantly violates the $\Omega_f - \bar{I} - \Lambda$ fits in Eqs. (18) and (19) to more than about 1%. Moderate deviations are limited to low-mass hybrid stars $\lesssim 1M_\odot$ with strong phase transitions. Fits for the real part of Ω_f are somewhat more accurate than for the imaginary part. For $\bar{I} \gtrsim 15$, i.e., $M \lesssim 1.6M_\odot$, the maximum deviation of the real part reduces to only 0.3%. Interestingly, the $\Omega_f - \Lambda$ relation is generally even more precise than for the $\Omega_f - \bar{I}$ relation except for low-mass configurations near $1M_\odot$. In hadronic NSs, the maximum deviation of the real (imaginary) part is about 0.2% (2%). The fits and maximum deviations from Refs. [7] (Lau), [10] (Chirenti), [9] (Chan), [11] (Lioutas), and [76] (Sotani), are also shown in Figs. 7 and 8. Lau used 9 hadronic EOSs and 2 quark EOSs. Lioutas used 20 hadronic EOSs. Sotani used 8 hadronic EOSs. Chirenti used 9 hadronic EOSs. Chan used 5 hadronic EOSs and 1 quark EOSs. Our work includes 2495 hadronic EOSs, 2189 hybrid NS EOSs and 20 quark EOSs. Our work thus demonstrates that these relations are truly universal.

VI. THE SPECIAL 1-NODE F-MODE BRANCH

The f-mode is characterized by the lowest radial order (n=0) for normal EOS. We found the f-modes of low-mass hybrid stars with strong phase transition that lead to the so-called twin star phenomenon can be qualitatively different than the normal f-modes. The twin star phenomenon is the situation where, as central density is increased through the phase transition density, the mass and radii both initially decrease. Such configurations are dynamically unstable. As the central density is further increased, the mass may begin to rise while the radius continues to fall, leading to a twin branch of stable configurations. Note that the normal and twin stable branches are disconnected in $M - R$ space. It is then possible to have stable stars with the same mass but differing radii (and also f-mode frequencies). Such a situation can be seen in Fig. 3 for a few cases, including $c_s^2 = 1, n_t = 2n_s$ and $\Delta\varepsilon/\varepsilon_t = 0.8$ (solid red curves in lowest panels). To demonstrate the different f-mode behavior on the more compact twin star branch, we utilize this particular EOS in Figs. 9 and 10.

In a normal star without a first-order transition, all perturbation amplitudes are continuous and smooth, see Fig. 14 or the top left panel of Fig. 9. In a hybrid star with a first-order transition, however, the slopes of all perturbation amplitudes become discontinuous, and V itself becomes discontinuous, at the transition boundary (last 7 panels of Fig. 9). For hybrid stars with relatively small quark cores that occupy the twin star branch, all fluid and metric perturbation amplitudes can become negative in some parts of the star between the phase transition and the surface (second through sixth panels of Fig. 9. The overall sign of the perturbations is trivial since we define a positive fluid perturbation amplitude $W = 1$ at the center of the NS. What's nontrivial is that the unstable and some stable hybrid stars have a radial node (zero) in the fluid and metric perturbation amplitudes X, W, H_0, H_1, K (but not V, which, however discontinuously changes sign) at a radius slightly larger than the phase transition radius R_t. We will call this type of behavior 1-node II (second through fourth panels of Fig. 9). The radial nodes move outward with increasing central density or pressure and R_t. Above some critical R_t, the radial nodes for X, W, H_0, H_1 and K simultaneously vanish, but the discontinuity and sign change in V remains (fifth and sixth panels of Fig. 9). Stars with radial nodes in V only we refer to as 1-node I. For hybrid stars with even larger cores, the discontinuity in V remains, but it no longer has a sign change at R_t, and the f-mode oscillations recover the standard $n = 0$ behavior of hadronic stars (last two panels of Fig. 9). Although V is always discontinuous at R_t, see Eq. (A4), the discontinuity magnitude becomes small for massive hybrid stars. The exotic behavior of the perturbation amplitudes causes f-mode frequencies of twin stars to somewhat deviate from universal relations for masses near M_t, see Fig. 10. A gap of about 0.1 kHz can appear in the f-mode frequency spectrum for $M \simeq M_t$. The f-mode frequencies and damping times of both 0-node and 1-node hybrid stars show deviations as well, see middle panels of Figs. 7 and 8. The f-mode frequency of hybrid NSs is not continuous between the 1-node I and 1-node II branches. The 1-node II branch side has a lower frequency than the 1-node I branch, and the damping time greatly increases near the critical point between 1-node I and 1-node II branches.

While the particular configurations explored here would never be expected to be observed because of the

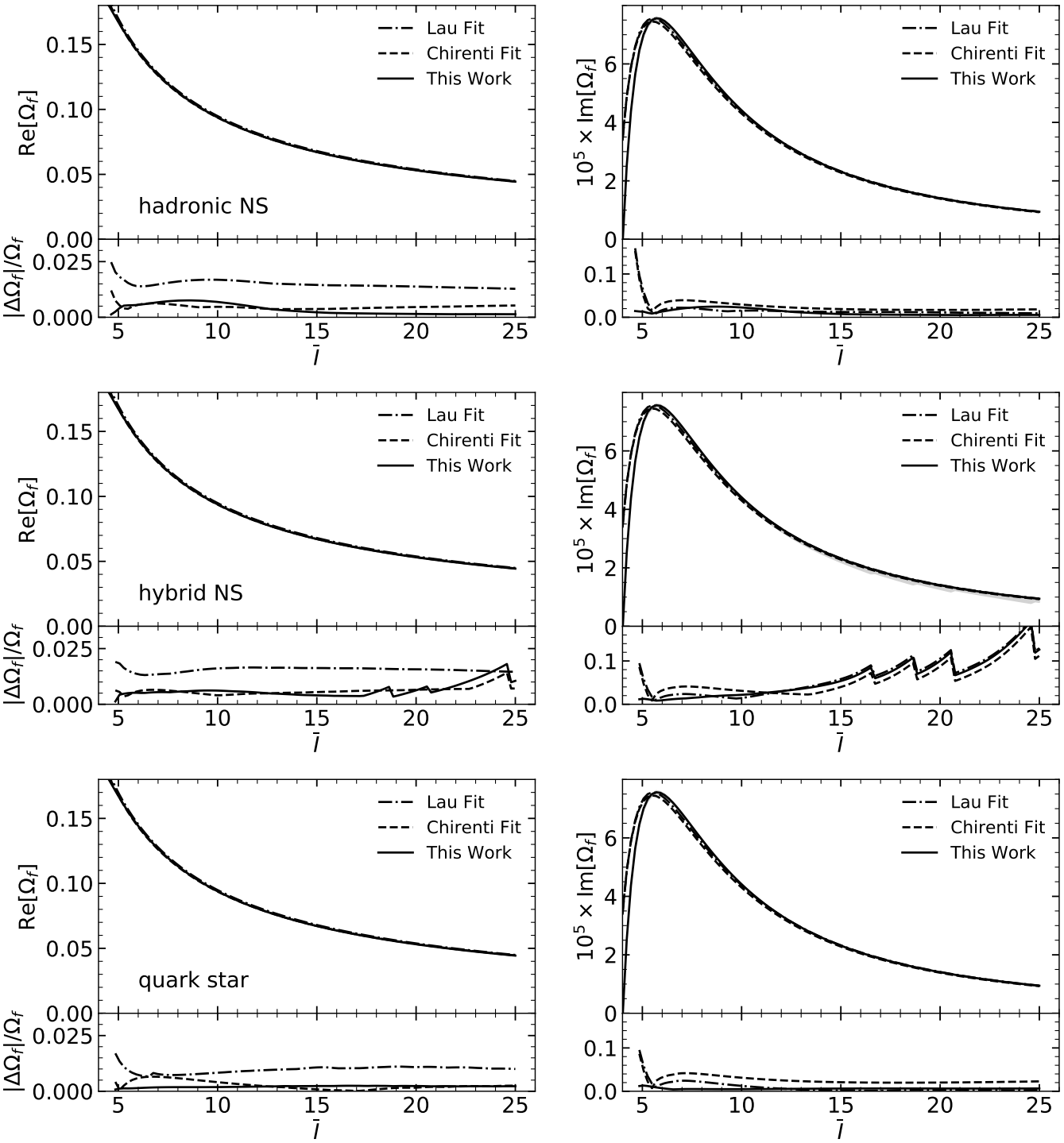

FIG. 7. The same as Fig. 6 except for the $\Omega_f - \bar{I}$ universal relation. "This Work" refers to Eq. (18) and other fits are due to Refs. [7] (Lau) and [10] (Chirenti) are shown.

small value of M_t, such behavior could have observational consequences for hybrid EOSs where $M_t \gtrsim 1M_\odot$. For example, the case $c_s^2 = 1, n_t = 4n_s$ and $\Delta\varepsilon/\varepsilon_t = 0.8$ shown in Fig. 3 (red dashed line in the bottom row) has a transition mass $M_t \simeq 1.6M_\odot$. But this case cannot be observationally realized since $M_{\rm max} \simeq 1.6M_\odot$ is too small. For the N3LO-cen and $\pm\sigma$ hadronic EOSs, which are relatively soft, we do not find it possible to produce twin stars simultaneously having $M \geq 1M_\odot$ and $M_{\rm max} \geq 2M_\odot$. It is possible, however, for these conditions to be realized for stiffer hadronic EOSs.

The models of Refs. [78] and [79] provide some exam-

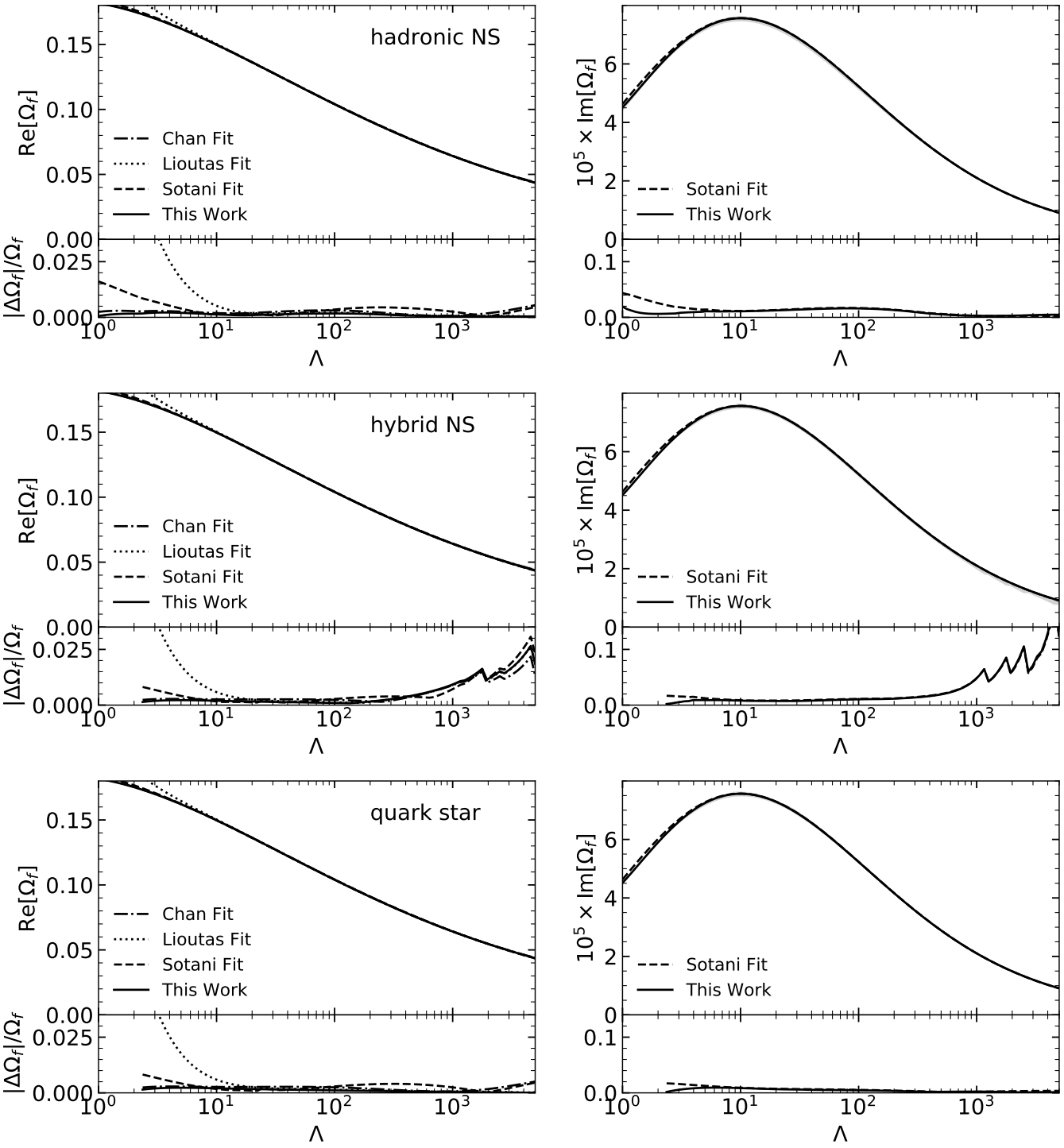

FIG. 8. The same as Fig. 6 but for the $\Omega_f - \Lambda$ universal relation. "This Work" refers to Eq. (19) and other fits due to Refs. [9] (Chan), [11] (Lioutas), and [76] (Sotani) are shown.

ples for stiffer EOSs which satisfy both constraints on the symmetry energy at saturation density and the inferred GW170817 tidal deformability. One caveat is that the quark matter part of the EOS must have $c_s^2 > 1/3$. The twin star cases in these studies are of two types, one having M_t below that of the largest component of GW170817 but $\geq 1M_\odot$, and the other having $M_t \gtrsim 2M_\odot$. The 1-node behavior might be potentially observable for these cases. In any event, our previously established universal relations can be accurately extended to hybrid stars,

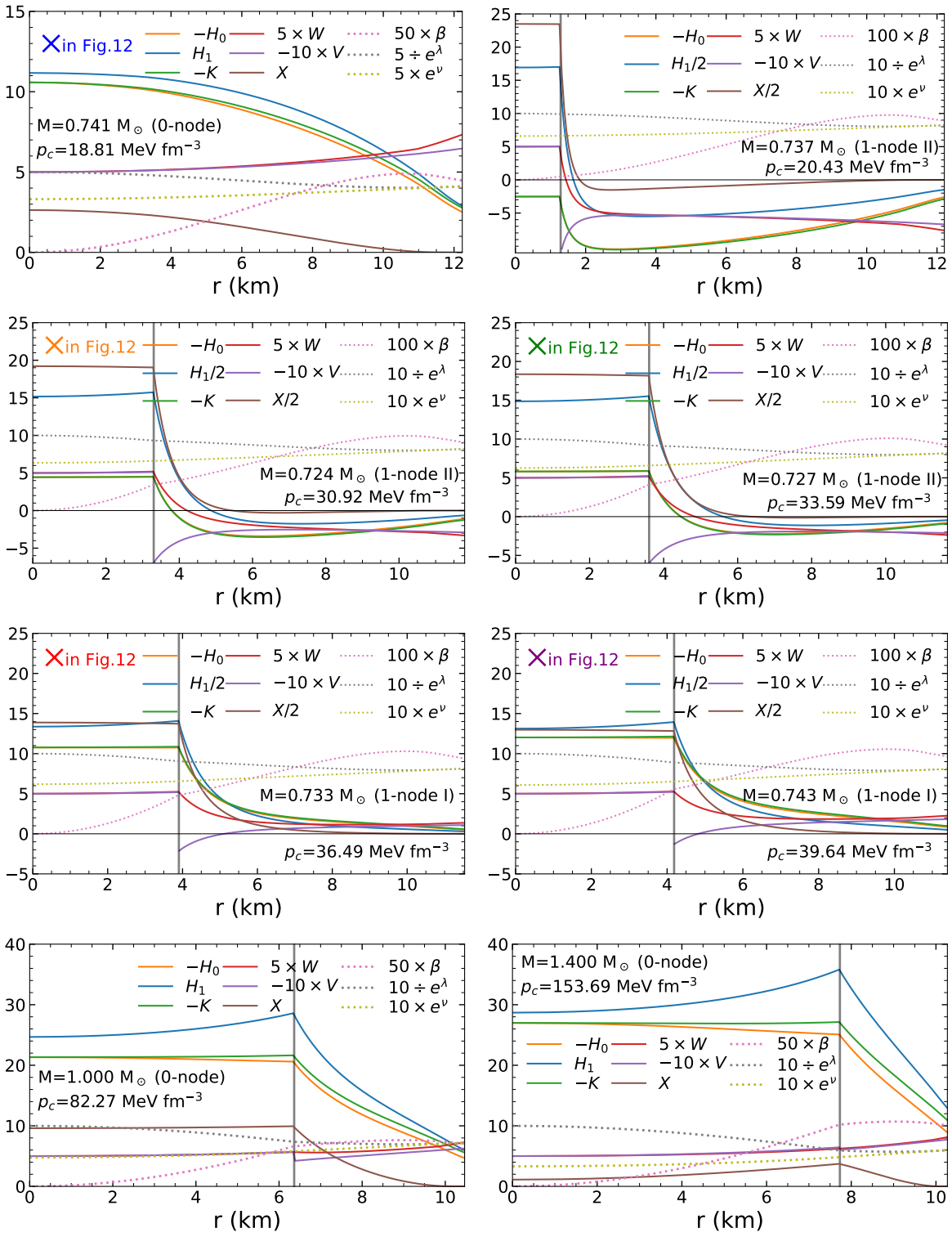

FIG. 9. Metric and real parts of fluid perturbation amplitudes (solid), and static metric functions (dotted) for the case of a hybrid star (except for the upper left panel where the central pressure equals the transition pressure, $p_c = p_t$). The phase transition is marked with a vertical solid line at $r = R_t$. Five of the panels have the same p_c as in Fig. 10 and are so indicated with colored crosses. H_0, H_1 and K are in units of $\varepsilon_s = 152.26$ MeV fm^{-3}, X is in units of ε_s^2 and W, V, λ and ν are dimensionless.

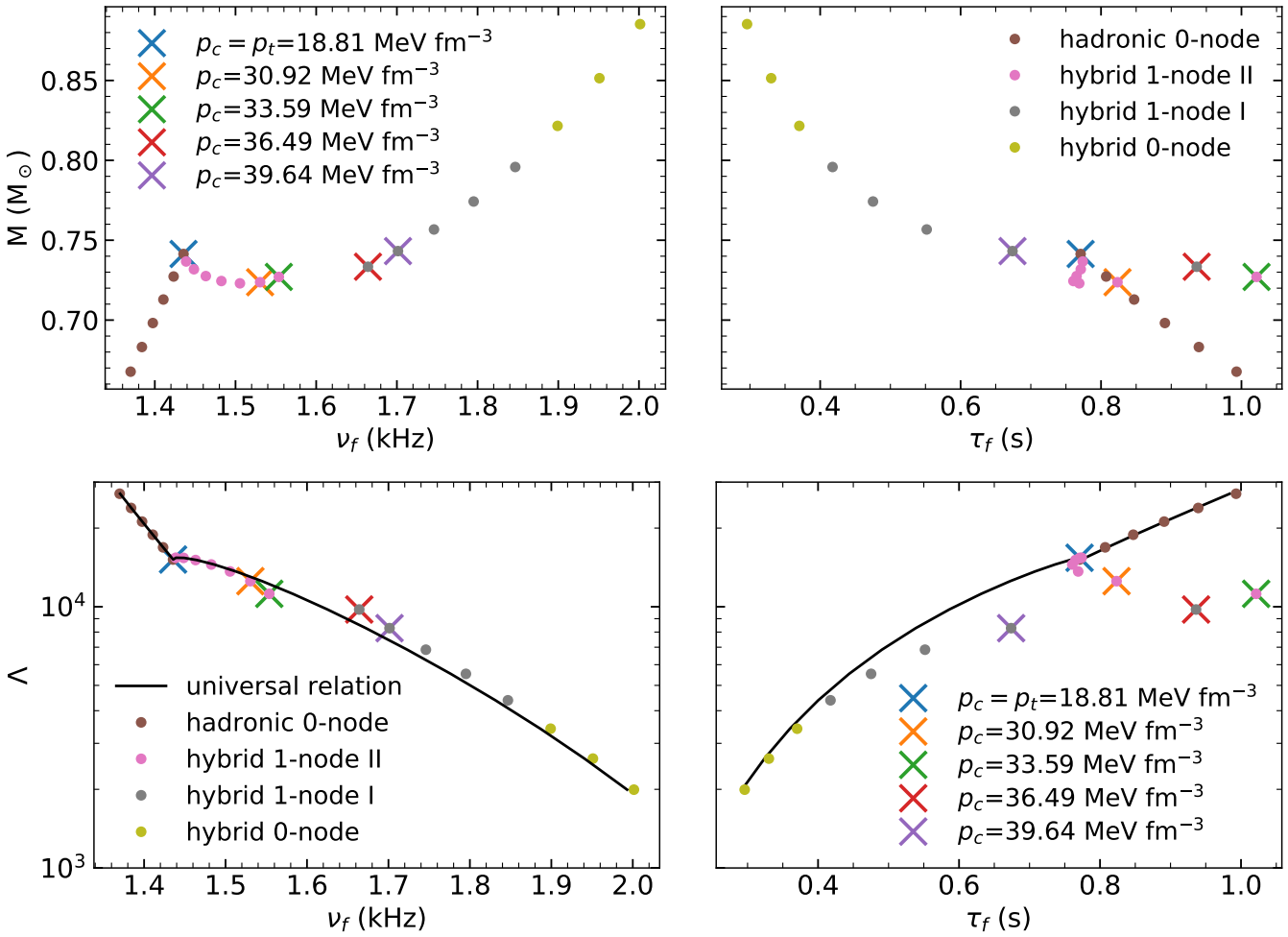

FIG. 10. f-mode frequency and damping time for hybrid NSs with small quark cores as functions of mass and tidal deformability. Brown and yellow dots represent stars with normal f-modes having no radial nodes, while pink and grey dots represent stars with the special 1-mode behavior. The colored crosses correspond to 5 configurations displayed in Fig. 9. In the tidal deformability plots, the universal relations from Eq. (19) are shown.

with small violations only in the case of twin stars with masses near M_t.

VII. THE DISCONTINUOUS G-MODE OF HYBRID NS

We are also interested in the g-mode that accompanies a discontinuity inside a NS. Since the EOSs of both strange quark stars and hadronic stars have no discontinuities, we focus on the discontinuous g-mode for hybrid stars described in Section III. For comparison purposes, we calculated g-mode frequencies with and without the Cowling approximation (left panel of Fig. 11). The relative error reaches 12% (22%) for $c_s^2 = 1/3$ ($c_s^2 \geq 1/3$). This error is significantly lower than that of the Cowling approximation for the f-mode. Considering that there's no universal relation accurate to the few percent level for the g-mode, the Cowling approximation could serve as a reasonable approximation. However, previous studies have been too optimistic about its accuracy, e.g. a claimed 5% error by Refs. [60] and [80]. This is due to our consideration of a wider variety of first order transitions, not just the relatively weak core-crust transition, as well as our inclusion of more realistic NSs ($M > 1.2M_\odot$).

Given that even the Cowling approximation involves a complex numerical calculation, it would be useful to find an analytic fit to the fully relativistic results. In Newtonian fluid mechanics, the frequency of surface gravity waves between two stratified fluids with a uniform gravitational field (i.e., the slab approximation) is analytically solvable [81]:

$$\omega_g^2 = \frac{(\varepsilon_+ - \varepsilon_-)gk}{\varepsilon_+/\tanh[kd_+] + \varepsilon_-/\tanh[kd_-]}, \qquad (20)$$

where g is the gravitational acceleration and k is the angular wave number. $\varepsilon_+ = \varepsilon_t + \Delta\varepsilon$ ($\varepsilon_- = \varepsilon_t$) and $d_+ = R_t$ ($d_- = R - R_t$) stand for the energy density and depth,

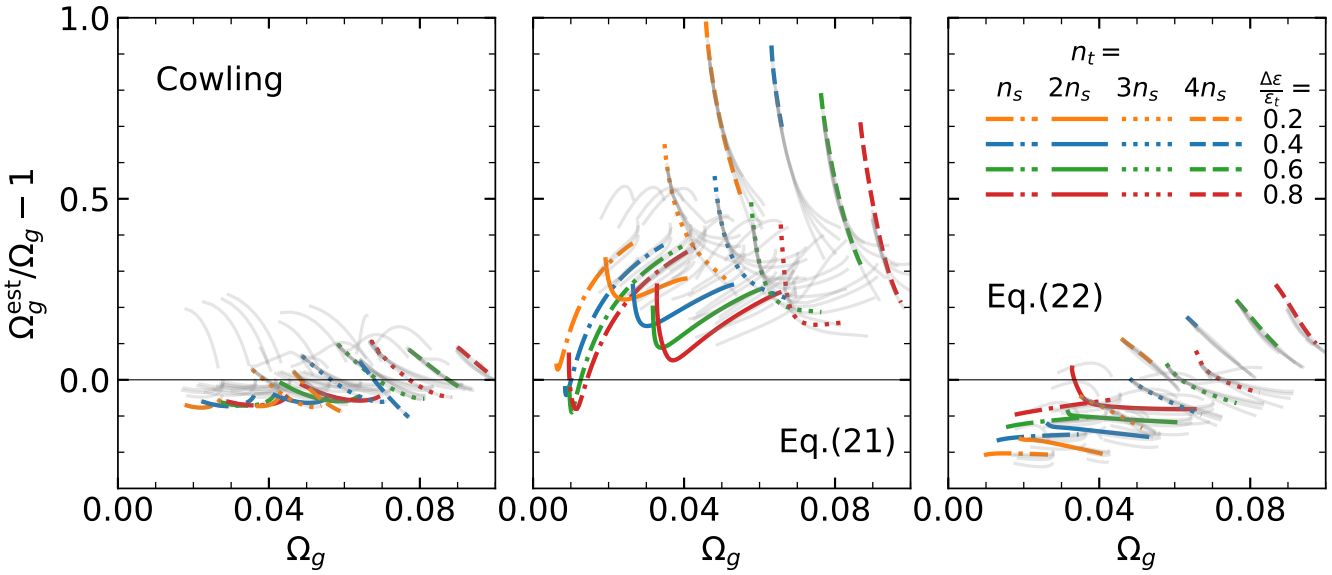

FIG. 11. Deviations of various estimations of g-mode frequencies from fully general relativistic calculations. The left, middle and right panels show the Cowling approximation and the fits of Eq. (21) and (22), respectively. Colored lines correspond to cases with $c_s^2 = 1/3$ while gray lines show results with higher values of c_s^2.

respectively, on the high (low) density side. When the discontinuity at R_t happens near the surface R of a star, the geometry approximates a stratified two-fluid problem with $k = \sqrt{l(l+1)}/R_t$. Red shifts in the frequency and gravitational acceleration approximately cancel, so g can be taken to be that of Newtonian gravity, GM_t/R_t^2. Ref. [80] concludes that discontinuous g-modes near the NS surface can be approximated, using $R - R_t << R_t$, $M - M_t << M_t$, and $\Delta\varepsilon << \varepsilon_t$, as

$$\Omega_g^2 \approx l(l+1)\beta^3 \frac{\Delta\varepsilon/\varepsilon_t}{1+\Delta\varepsilon/\varepsilon_t}(1 - R_t/R). \qquad (21)$$

We tested this approximation with $\ell = 2$ and find relatively large deviations, see the middle panel of Fig. 11, partly because their assumption of infinite depth $d_+ >> d_-$ breaks down for $R_t/R < 0.5$ [65]. Instead, we don't assume $\Delta\varepsilon << \varepsilon_t$, $M - M_t << M_t$ or $R - R_t << R_t$, and we also approximate the wave number with $k = D/R_t$, where the fitting parameter $D = 1.21$. This leads to

$$\Omega_g^2 \approx \frac{\beta^3 (M_t/M)(R/R_t)^3 (\Delta\varepsilon/\varepsilon_t) D \tanh[D]}{1+\Delta\varepsilon/\varepsilon_t + \tanh[D]/\tanh[D(R/R_t - 1)]}, \qquad (22)$$

which performs significantly better than Eq. (21) and comparably to the Cowling approximation, see Fig. 11. We note this fit for the g-mode frequency depends only on $M/R, M_t/M, R_t/R$ and $\Delta\varepsilon/\varepsilon_t$ and is otherwise insensitive to the hybrid EOS parameters ε_t and c_s as well as the assumed hadronic EOS.

Fig. 12 shows the mass dependence of the g-mode frequency and damping time with various high-density sound speeds, transition densities and density discontinuities. In most cases for stable NSs, g-mode frequencies are not very sensitive to NS mass. However, damping times have a very strong mass dependence. Both very low and very high mass hybrid NSs have relatively long damping times. A previous study with a different EOS parameterization suggested that g-mode damping times are significantly larger than those of other damping mechanisms [65]. Our calculation shows smaller g-mode damping times. When the density discontinuity approaches $\Delta\varepsilon/\varepsilon_t = 1$, g-mode damping times become comparable to the neutrino damping time, $0.1 - 10$ s [82]. However, these configurations have relatively low $M_{\rm max}$. If we impose $M_{\rm max} > 2M_\odot$ and causality constraints, the discontinuous g-mode damping times should satisfy $\tau_g \gtrsim 10^6$ s.

Eq. (22) is based on Newtonian mechanics and provides a reasonable but coarse approximation. Starting from the fact that the g-mode frequency is relatively insensitive to the neutron star mass (Fig. 12), we focus on the g-mode frequencies of maximum mass hybrid NS configurations, which are shown in Fig. 13 for different values of c_s, $\Delta\varepsilon/\varepsilon_t$ and n_t. If we impose $M_{max} > 2M_\odot$ and causality constraints, the discontinuous g-mode frequency satisfies $\nu_g \lesssim 1.25$ kHz. g-modes of observed stars will be at slightly larger frequencies than those shown in Fig. 13 for a given set of quark star parameters.

VIII. DISCUSSION AND CONCLUSION

With the improvement provided by the next generation of gravitational-wave telescopes, we may detect gravitational waves from quasi-normal modes of NS oscillation.

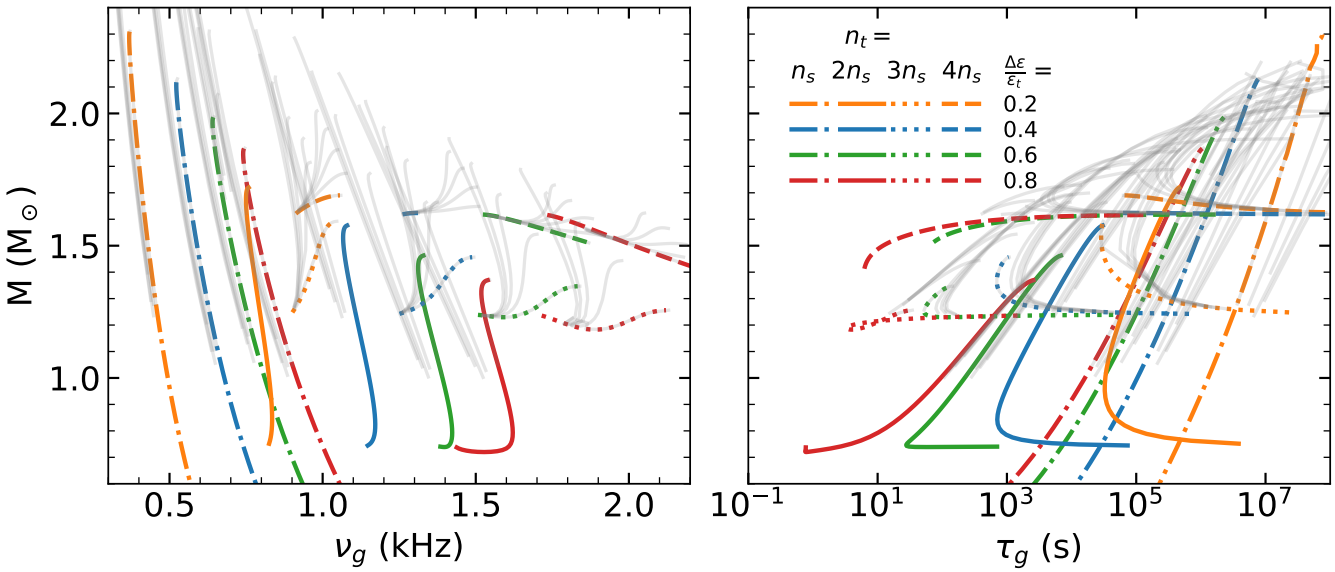

FIG. 12. The left (right) panel shows the g-mode frequency (damping time) versus mass for hybrid NSs modeled with χEFT and the *CSS* parameterization. Colored lines correspond to cases with $c_s^2 = 1/3$ while gray lines show results with higher values of c_s^2.

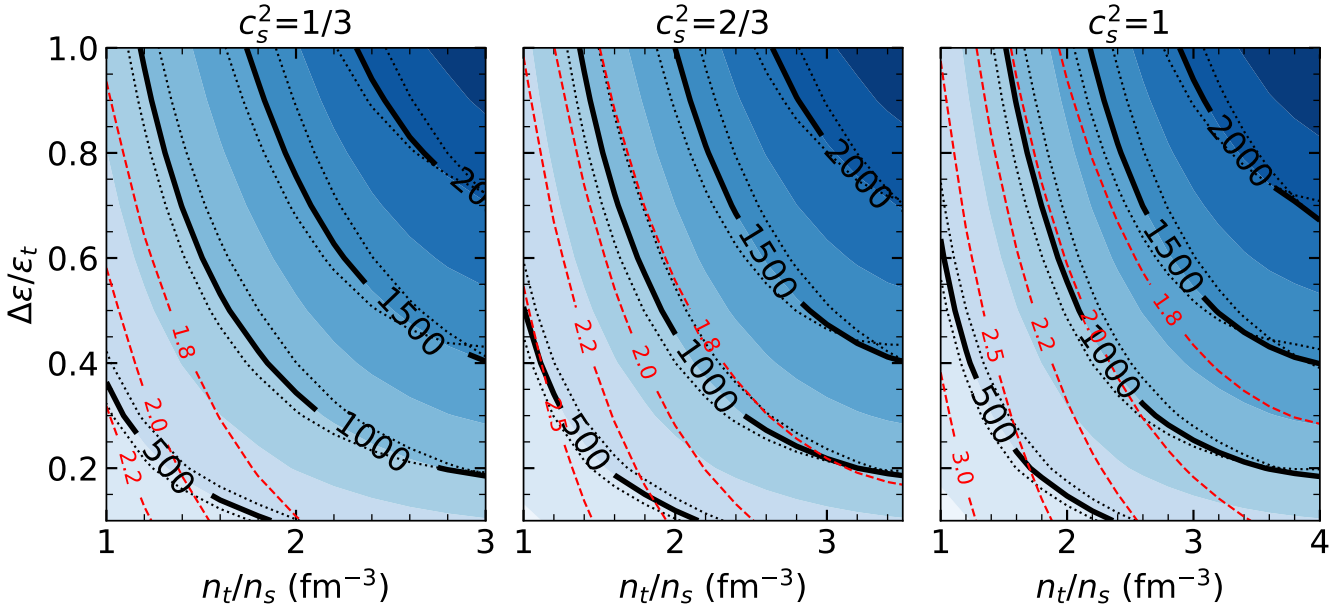

FIG. 13. The g-mode frequencies $\nu_{g,\max}$ of maximum mass hybrid configurations are shown as black contours using the hadronic N3LO-cen chiral EFT EOS, with dotted lines representing the $\pm\sigma$ uncertainties in the hadronic EOS. Intermediate frequency values are indicated by blue shading. Red contours indicate $M_{\max}$.

In this paper, we focus on the f-mode and the discontinuity g-mode oscillations, which have frequencies in the detectable range. The f-mode has a relatively large coupling with tidal excitations, while the discontinuity g-mode has a lower frequency that would be excited earlier in the inspiral stage of a BNS merger and which would give a larger phase shift due to the additional orbital momentum decay.

The NS oscillations were calculated using three methods. In asteroseismology, fluid oscillations, including g-, f- and p-modes, have been extensively studied in Newtonian gravity [1]. In compact object where general relativistic effects are important, the canonical ODEs for non-radial oscillation were proposed by [2] and reformu-

lated by Refs. [3, 47] in full general relativity and by Ref. [55] utilizing the relativistic Cowling approximation.

We first compared Newtonian calculations with both the widely-used relativistic Cowling approximation and the linearized relativistic formulation for the f-mode of 3 analytic solutions and also the SLy4 EOS. Due to the finite densities at the NS surface, the analytic incompressible (Inc) solution is manifestly different from those of the analytic Tolman VII (T VII) and Buchdahl (Buch) as well as the SLy4 EOS. Although both the Newtonian and approximate Cowling calculations tend to overestimate f-mode frequencies, the Newtonian calculation performs extremely well in low mass NSs and better than the Cowling approximation in canonical mass NSs. However, the Newtonian approximation becomes worse than the Cowling approximation in the highest mass NSs. This is reasonable since the Newtonian calculation keeps gravitational perturbations, which the Cowling approximation ignores. However, for massive and extremely compact NSs, relativistic corrections overwhelm the corrections due to gravitational perturbations. Since we require accurate results to formulate EOS-insensitive and quasi-universal relations with the compactness, tidal deformability and/or moment of inertia, further calculations are only performed in the full linearized general relativistic limit.

Previous work has studied f-mode frequencies and damping times, and proposed EOS-insensitive correlations with compactness β and tidal deformability Λ, of both hadronic and pure quark (self-bound) stars for a relatively few number of EOSs. We have checked these formulae for a much more exhaustive sampling of equations of state employing a piecewise polytrope scheme to model high densities, and proposed more accurate correlations. In addition, we extended these studies to hybrid stellar configurations consisting of quark cores and hadronic exteriors, showing that correlations established for purely hadronic stars also fit general hybrid configurations. Always enforcing both causality and lower and upper maximum mass limits (i.e., $2M_\odot < M_{\rm max} < 2.6M_\odot$), f-mode frequencies lie in the range 1.3-2.8 kHz and damping times in the range 0.1-1 s for all configurations. The f-mode frequency of pure quark stars with canonical masses depends relatively weakly on mass, similarly to the mass-dependence of the radius of hadronic NSs. Whereas the f-mode frequencies of hadronic NSs increase smoothly with mass, hybrid NSs with strong first order transitions can result in twin star configurations which have different f-mode frequencies for the same mass. We note that low mass stars (≈ 1 M$_\odot$) with high f-mode frequencies ($f \gtrsim 2.1$ kHz) can only be achieved without the existence of a crust, i.e., only for self-bound (pure quark) stars, just as the radius of a $1M_\odot$ NS with a normal crust cannot be smaller than ≈ 10.5 km given constraints from the PNM calculation. Note that this bounds depends weakly on the choice of EOS parameterizations. By exploring parameterizations other than *PP3*, we found it might be lowered to 10.2 km. If such large frequencies are observed, it would be an indication of a very small radius, and evidence for the existence of pure quark stars.

Employing a range of parameterizations covering the allowed physical limits, we find that the dimensionless f-mode frequency is proportional to $\beta^{5/4}$ for hadronic and hybrid NS. In contrast, pure quark stars follow $\Omega_f \propto \beta^{3/2}$ which is found for analytic solutions in the Newtonian approximation. These scalings are shown to be accurate to about the 8% level, but more accurate power-law fits for all three types of stars are given. Although our fits to hadronic and hybrid stars are of similar accuracy to previous work, we verified their applicability to a much broader range of underlying EOSs. Our fits for quark stars, in addition, are superior to previous work.

We verified that the f-mode and its damping time correlate even more strongly (to better than 1% accuracy) with higher-order radial moments of NSs compared to β, even for hybrid and pure quark stars. These correlations with higher order moments are known as the $\bar{I} - \Lambda - \Omega_f$ relations [7]. We found that the $\Lambda - \Omega_f$ correlation is slightly more accurate than the $\bar{I} - \Omega_f$ correlation, reaching 0.1% accuracy for low mass hybrid stars with large quark cores. Our fitting formulae have similar accuracy to previous works but are applicable to wider range of NS masses and much larger samples of EOSs.

We discovered an abnormal f-mode in hybrid NSs displaying the twin star phenomenon with central pressures just above the quark-hadron transition pressure p_t. These exhibit manifestly different profiles of fluid and metric perturbation amplitudes. Canonical f-modes have no nodes for both fluid and metric perturbation amplitudes, e.g. Fig. 14, left upper panel, and Fig. 9, lower two panels. As the quark core first develops, the amplitude V becomes discontinuous and flips its sign at the quark-hadron interface, while the amplitudes H_0, X and W form nodes close to the interface (the 1-node II state). With increasing central pressure and quark core size, the nodes in H_0, X and W eventually disappear, while V simultaneously forms a node (the 1-node I state. Further increases in central pressure lead to the disappearance of the node in V and normal 0-node behavior is restored. However, directly probing number of nodes is impossible at present. The only potential observable is its eigenfrequency. In both 1-node cases, the f-mode frequency moderately deviates from the $\bar{I} - \Lambda - \Omega_f$ universal relation (the only significant violations we have found), and also a gap forms in the f-mode frequency spectrum. This might provide an opportunity to directly observe the existence of a strong first order transition. Although the examples studied in this paper are limited to the unobservable range $M_t < 1M_\odot$, it is remotely possible that a stiffer EOS above about $1.5 - 2n_s$ could provide suitable conditions for obtaining the twin star phenomenon with $M_t > 1M_\odot$. To our knowledge, we are the first to report the existence of this special 1-node behavior of the f-mode.

The discontinuous g-mode frequency (which requires the existence of a discontinuity in the density) depends

strongly on the magnitudes of both the transition density and its discontinuity. On the other hand, for a given set of EOS parameters, it depends weakly on the stellar mass. Uncertainties in the low-density hadronic EOS contribute less than about 5% uncertainty to the g-mode frequency. Due to causality and maximum mass constraints, the discontinuous g-mode frequency has an upper bound of about 1.5 kHz. However, if the squared sound speed in the inner core is restricted to $c_s^2 \leq 1/3$, the discontinuous g-mode can only reach about 0.8 kHz, which is significantly lower than the f-mode frequency of 1.3-2.8 kHz. Also, in this eventuality, the g-mode gravitational wave damping time is usually extremely long, being larger than 10^4 s compared to about 10^2 s for an inner core in which $c_s^2 \leq 1$, and is also large compared with the usual f-mode damping time, 0.1-1 s. We found an improved analytic fit for the g-mode frequency that depends only on $M/R, M_t/M, R_t/R$ and $\Delta\varepsilon/\varepsilon_t$ and which is otherwise insensitive to the hybrid EOS parameters ε_t and c_s^2 as well as the assumed hadronic EOS. We found the Cowling approximation is accurate to within 20%, which is significantly less accurate than previously estimated, due to our consideration of a larger variety of first order transitions and realistic NS masses. Our analytic approximation has a similar accuracy. We also established a more accurate fit based on M_{max} stars that depends on $p_t, \Delta\varepsilon/\varepsilon_t$, and c_s, and showed that for physically plausible situations, $\nu_g < 1.25$ kHz.

In this work, we assume the perturbed fluid is ideal. Superfluidity inside the NS introduces an additional flow component which is discussed in other works, such as Ref. [83]. The fluid perturbations are also assumed to be barotropic, which holds only when matter is adiabatic and always in equilibrium except for the phase conversion between quarks and hadrons. However, we checked in some typical cases where a phase transition occurs in a hybrid star [15], a non-barotropic EOS involving composition or temperature gradients does not lead to substantial modification of our present results for frequencies and damping times of f-modes. Non-adiabatic effects, such as from the neutrino Urca processes during the inspiral and merger phases, could introduce significant additional damping due to bulk viscosity [84, 85].

ACKNOWLEDGMENTS

T.Z is supported by the U.S. DOE Grant No. DE-FG02-93ER40756. J.M.L. and T.Z. acknowledge support by the U.S. DOE under Grant No. DE-FG02-87ER40317 and by NASA's NICER mission with Grant 80NSSC17K0554.

Appendix A: Oscillation Frequencies and Damping Times

Thorne et. al. first studied NS oscillations coupled with gravitational radiation [2]. Oscillations of NS are expected to involve linear variations of matter and metric in various spherical harmonics. The angular decomposition of variations will contain even and odd parity components. Odd parity variations have a trivial zero mode which corresponds to differential rotation, unless axial symmetry is broken by rotation which result in r-modes [86]. In this work, we study only even parity perturbation of the Regge-Wheeler metric,

$$\begin{aligned} ds^2 = &-e^{\nu(r)}(1 + r^\ell H_0(r) e^{i\omega t} Y_{\ell m}(\phi,\theta))c^2 dt^2 \\ &+e^{\lambda(r)}(1 - r^\ell H_0(r) e^{i\omega t} Y_{\ell m}(\phi,\theta))dr^2 \\ &+(1 - r^\ell K(r) e^{i\omega t} Y_{\ell m}(\phi,\theta))r^2 d\Omega^2 \\ &-2i\omega r^{\ell+1} H_1(r) e^{i\omega t} Y_{\ell m}(\phi,\theta) dt dr \end{aligned} \tag{A1}$$

where H_0, H_1, and K are metric perturbation functions. ω is the complex oscillation frequency; its real component is the oscillation frequency and its imaginary component is the inverse of the damping (growth) time if it's positive (negative). The metric perturbation functions inside the star must match those outside the star at the stellar surface.

1. Perturbations inside the NS

Fluid perturbation vectors inside the star can be decomposed in a basis of spherical harmonics in terms of Y_m^ℓ, $\partial_\theta Y_m^\ell$ and $\partial_\phi Y_m^\ell$. For non-rotating neutron stars, odd parity fluid perturbations have a trivial solution which corresponds to differential rotation, while fluid perturbations with even parity are described by the Lagrangian displacement vectors

$$\begin{aligned} \xi^r &= r^{\ell-1} e^{-\lambda/2} W Y_m^\ell e^{i\omega t} \\ \xi^\theta &= -r^{\ell-2} V \partial_\theta Y_m^\ell e^{i\omega t} \\ \xi^\phi &= -\frac{r^{\ell-2}}{\sin^2\theta} V \partial_\phi Y_m^\ell e^{i\omega t}, \end{aligned} \tag{A2}$$

which define the fluid perturbation amplitudes W and V. In case of radial oscillations when $\ell = 0$, the angular fluid perturbation V is irrelevant due to the vanishing of ∂_θ and ∂_ϕ. Perturbations of a spherical star have four degrees of freedom: three coming from the metric perturbations, which will be reduced by one applying Einstein's equation, $\delta G^{01} = 8\pi\delta T^{01}$, and two coming from fluid perturbations. An additional fluid perturbation amplitude X , related to Lagrangian pressure variations, is defined according to

$$\Delta p = -r^\ell e^{-\nu/2} X Y_m^\ell e^{i\omega t}. \tag{A3}$$

In order to avoid potential singularity in the eigenvalue problem, Lindblom et. al. pick the four independent

variables to be H_1, K, W, X [3, 47] and evaluate the two remaining functions H_0 and V according to

$$H_0 = \left\{8\pi r^2 e^{-\nu/2} X - \left[(n+1)\mathrm{Q} - \omega^2 r^2 e^{-(\nu+\lambda)}\right] H_1 + \left[n - \omega^2 r^2 e^{-\nu} - \mathrm{Q}(\mathrm{Q}e^{\lambda} - 1)\right] K\right\} (2b + n + \mathrm{Q})^{-1},$$
$$V = \left[\frac{X}{\varepsilon + p} - \frac{\mathrm{Q}}{r^2} e^{(\nu+\lambda)/2} W - e^{\nu/2}\frac{H_0}{2}\right] \frac{e^{\nu/2}}{\omega^2}, \qquad \text{(A4)}$$

where $n = (\ell-1)(\ell+2)/2$, $Q = b + 4\pi G r^2 p/c^4$ and $b = Gm/(rc^2)$ with $m(r)$ the mass interior to r. By expanding Einstein's equation to first-order, homogeneous linear differential equations for H_1, K, W and X can be found [47],

$$\begin{aligned} r\frac{dH_1}{dr} &= -\left[l + 1 + 2be^{\lambda} + 4\pi r^2 e^{\lambda}(p - \varepsilon)\right] H_1 \\ &\quad + e^{\lambda}\left[H_0 + K - 16\pi(\varepsilon + p)V\right], \\ r\frac{dK}{dr} &= H_0 + (n+1)H_1 \\ &\quad + \left[e^{\lambda}Q - \ell - 1\right] K - 8\pi(\varepsilon + p)e^{\lambda/2} W, \\ r\frac{dW}{dr} &= -(\ell+1)\left[W + \ell e^{\lambda/2} V\right] \\ &\quad + r^2 e^{\lambda/2}\left[\frac{X}{(\varepsilon+p)c_s^2} e^{-\nu/2} + \frac{H_0}{2} + K\right], \end{aligned} \qquad \text{(A5)}$$

$$r\frac{dX}{dr} = -\ell X + \frac{\varepsilon + p}{2} e^{\nu/2}\left\{(3e^{\lambda}Q - 1)K - \frac{4(n+1)e^{\lambda}Q}{r^2} V + (1 - e^{\lambda}Q)H_0 + (r^2\omega^2 e^{-\nu} + n + 1)H_1 + \left[2\omega^2 e^{\lambda/2-\nu} - 8\pi(\varepsilon + p)e^{\lambda/2} + r^2\frac{d}{dr}\left(\frac{e^{-\lambda/2}}{r^2}\frac{d\nu}{dr}\right)\right] W\right\}.$$

where the adiabatic sound speed c_s of NS matter under oscillation is different from the equilibrium sound speed c_e[13, 14]. Here, we only consider zero-temperature EOSs without varying chemical composition, so that $c_s = c_e$. The central boundary conditions for the perturbation amplitudes are

$$\begin{aligned} W(0) &= 1, \\ X(0) &= (\varepsilon_0 + p_0)e^{\nu_0/2} \times \\ &\quad \left\{\left[\frac{4\pi}{3}(\varepsilon_0 + 3p_0) - \frac{\omega^2}{\ell} e^{-\nu_0}\right] W(0) + \frac{K(0)}{2}\right\}, \\ H_1(0) &= \frac{\ell K(0) + 8\pi(\varepsilon_0 + p_0)W(0)}{n+1}. \end{aligned} \qquad \text{(A6)}$$

where $\nu_0 = \nu(0)$ and the last boundary condition is achieved by solving the two trial solutions with $K(0) = \pm(\varepsilon_0 + p_0)$ and then linearly constructing the correct solution satisfying the outer boundary condition $X(R) = 0$ (corresponding to no pressure variations at the surface). Note that $H_0(0) = K(0)$ by construction. For a hybrid NS (see Section III), we assume no chemical changes at the transition boundary [80, 87]. Thus, H_1, K, W, X should all be continuous at the transition, while H_0 and V are fixed by Eq. (A4). In this paper, we confine the remainder of our discussion to non-radial oscillations with $\ell = 2$, so that V and W, which are defined only inside a star, are dimensionless functions.

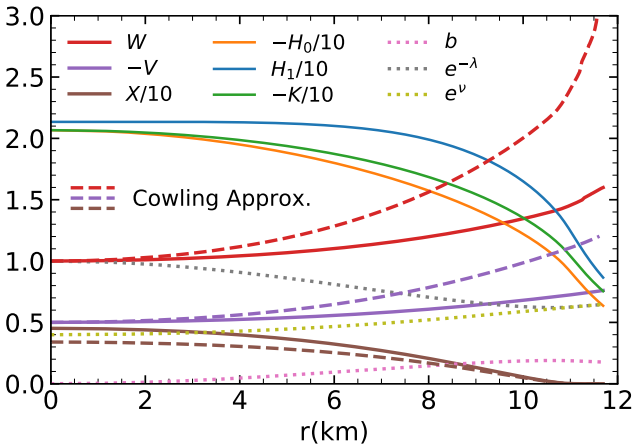

FIG. 14. Metric perturbation amplitudes, fluid perturbation amplitudes for non-radial oscillations with $\ell = 2$ with (dashed curves) and without (solid curves) the Cowling approximation, and static metric functions (dotted curves) inside a $1.4M_\odot$ NS computed with the Sly4 EOS [88]. H_0, H_1 and K are in units of $\varepsilon_s = 152.26$ MeV fm^{-3}, X is in units of ε_s^2, and W, V, ν and λ are dimensionless. Only real parts of the perturbation amplitudes are plotted.

As an example, Fig. 14 shows the static and metric perturbation amplitudes inside a $1.4M_\odot$ NS using the SLy4 EOS. The central pressure is $p_c = 85$ MeV fm^{-3}, the radius is $R_{1.4} = 11.72$ km, and the corresponding f-mode frequency is $\omega = (1.2146 \times 10^4 + 5.206i)$ s^{-1}, determined as in Sec. A 2. Since the imaginary part of the perturbation is very small compared with the real part, Fig. 14 shows only the real parts of the perturbation amplitudes. The Cowling approximation gives $\omega = 1.5130 \times 10^4$ s^{-1}, about 25% larger. The fluid perturbation amplitudes with the Cowling approximation are in error by up to a factor of 2 at stellar surface for W and V, and by about 25% at the center for X, as shown in Fig. 14.

Outside the NS, Eq. (A5) reduces to 2 first-order equations for H_1 and K; W and V are not defined in this region. These equations can be reformulated into a single Schrodinger-like equation known as the Zerilli equation,

$$d^2Z/dr^{*2} = (V_Z(r) - \omega^2)Z, \qquad \text{(A7)}$$

by defining [89]

$$\begin{pmatrix} K(r) \\ H_1(r) \end{pmatrix} = \begin{pmatrix} g(r) & 1 \\ h(r) & k(r) \end{pmatrix} \begin{pmatrix} Z(r^*)/r \\ dZ(r^*)/dr^* \end{pmatrix},$$
$$g(r) = \frac{n(n+1)+3nb+6b^2}{(n+3b)}, \quad \text{(A8)}$$
$$h(r) = \frac{(n-3nb-3b^2)}{(1-2b)(n+3b)},$$
$$k(r) \equiv \frac{dr^*}{dr} = \frac{1}{1-2b},$$

and an effective potential

$$V_Z(r) = (1-2b)\frac{2n^2(n+1)+6n^2b+18nb^2+18b^3}{r^2(n+3b)^2}. \quad \text{(A9)}$$

Note that here $b = GM/(c^2r)$ since $m(r>R) = M$. H_0 can be fixed by a simplified form of the last of Eq.(A4),

$$H_0 = \frac{\left[\omega^2r^2-(n+1)b\right]H_1 + \left[n(1-2b)-\omega^2r^2+b(1-3b)\right]K}{(1-2b)(3b+n)}. \quad \text{(A10)}$$

Fig. 15 shows the metric perturbation amplitudes outside the NS modeled in Fig. 14. In the far-field limit, the solution becomes that of oscillating gravitational radiation. The behavior of the metric perturbation amplitudes shown in Figs. 14 and 15 is generic for f-mode (n=0) and relatively insensitive to the EOS.

2. Determining the oscillation frequency

Our goal is to find the frequencies of eigenmodes that correspond to oscillations. The lowest order mode corresponds to the f-mode generally with zero node, while solutions of higher radial nodes correspond to the g- and p- modes. All the mode solutions should satisfy the correct boundary condition at infinity should be 'free', in other words, at infinity, the gravitational radiation field should be purely outgoing. We solve the Zerilli equation for $r \le 25\omega^{-1}$, which is found to be adequate. For larger r, the solution of Zerilli equation Z can be decomposed into incoming (Z_+) and outgoing (Z_-) radiation as

$$\begin{pmatrix} Z(\omega) \\ dZ/dr^* \end{pmatrix} = \begin{pmatrix} Z_-(\omega) & Z_+(\omega) \\ dZ_-/dr^* & dZ_+/dr^* \end{pmatrix} \begin{pmatrix} A_-(\omega) \\ A_+(\omega) \end{pmatrix},$$
$$Z_- = e^{-i\omega r^*}\left[\alpha_0 + \frac{\alpha_1}{r} + \frac{\alpha_2}{r^2} + \mathcal{O}(r^{-3})\right],$$
$$\frac{dZ_-}{dr^*} = -i\omega e^{-i\omega r^*}[\alpha_0 + \frac{\alpha_1}{r} \quad \text{(A11)}$$
$$+ \frac{\alpha_2 + i\alpha_1(1-2b)/\omega}{r^2} + \mathcal{O}(r^{-3})],$$
$$\alpha_1 = \frac{-i(n+1)\alpha_0}{\omega},$$
$$\alpha_2 = \frac{[-n(n+1)+iM\omega(3/2+3/n)]\alpha_0}{2\omega^2},$$

where $A_+(\omega)$ and $A_-(\omega)$ are the amplitudes of incoming and outgoing radiation, respectively, Z_+ is the complex conjugate of Z_-. The amplitude of incoming radiation $A_+(\omega)$ vanishes for physical eigenmodes. α_0 can be any complex number which represent an overall phase.

In order to determine ω, we need to solve for the root of $A_+(\omega) = 0$ in the complex plane. A straightforward, but inefficient, way would be to use a complex root finding algorithm. With the help of EOS-insensitive relations between $\nu = \mathrm{Re}[\omega]/(2\pi)$ and the moment of inertia (see Section V), three digits accuracy can be achieved for the f-mode within 8 Newton–Raphson iterations. Other techniques are needed to guess initial estimates for p- and g-modes. Note that the imaginary part of the eigenfrequency is usually small ($< 1/1000$ the magnitude of the real part) for f-, g- and p-modes. As a result, $\mathrm{Im}[Z(r^*)] << \mathrm{Re}[Z(r^*)]$ as well. Therefore, it's possible to approximately determine the complex eigenfrequency by approximating complex A_+ near the eigenfrequency with

$$A_+(\omega) \approx A_0 + A_1\omega + A_2\omega^2 = 0, \quad \text{(A12)}$$

where A_0, A_1 and A_2 are complex constants fixed by $A_+(\omega)$ along the real axis of ω. Solving this quadratic equation gives an estimate for the real and imaginary parts of eigenfrequency. This method avoids using a complex root-finding algorithm and is considerably more efficient.

Another simplified method to evaluate eigenmodes is to use the WKB approximation [4, 90]. The outside solution is approximated by a WKB wave-function. Perturbation functions near the NS surface can be used to fix amplitude of incoming and outgoing radiation without solving the Zerilli equation. We have verified that these two approximate methods agreed very well for low-damping modes where the imaginary part is small compared with the real part. Here, we use the interpolation method to determine an initial guess for ω to be used in the full solution.

Fig. 1 shows the f-mode frequency for the SLy4 EOS used in Figs. 14 and 15 as a function of neutron star compactness β. Note the approximately linear behavior with $\beta^{3/2}$, a universal scaling that becomes apparent

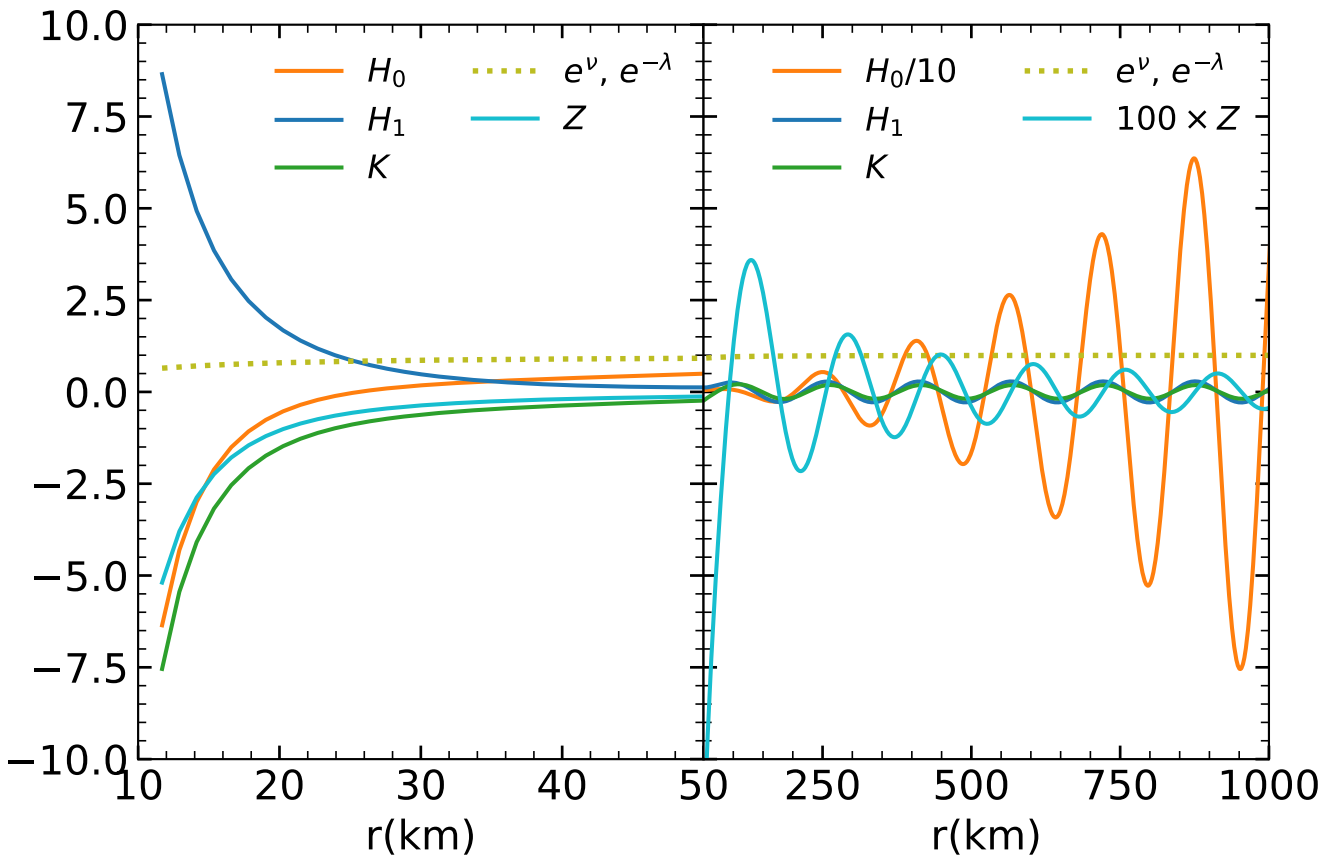

FIG. 15. The same as Fig. 14 except outside the $1.4M_{\odot}$ SLy4 EOS NS. Note the change of scale at $r = 50$ km.

when examining analytic results in Newtonican geometry with simple EOSs, as discussed in the next section.

A widely used approximation in the calculation of oscillation frequencies, the Cowling approximation, ignores the metric perturbation K, H_1 and H_2 in Eqs. (A4) - (A6). This reduces the 4 complex first-order ODEs Eqs. (A5) to 2 real first-order ODEs and results in no gravitational radiation damping, see Eqs. (19) and (20) in Ref. [15]. In addition, in this approximation the Zerilli equation for metric perturbations outside the NS, Eq. (A7), can be ignored which greatly simplifies the calculation. However, since the Cowling approximation introduces f-mode frequency errors of up to 30% [91], as shown in Fig. 1, it is not suitable for the study of the high accuracy universal relations sought in this work.

[1] J. P. Cox, *Theory of Stellar Pulsation.(PSA-2), Volume 2* (Princeton University Press, 2017).
[2] K. S. Thorne and A. Campolattaro, The astrophysical journal **149**, 591 (1967).
[3] L. Lindblom and S. L. Detweiler, The Astrophysical Journal Supplement Series **53**, 73 (1983).
[4] K. D. Kokkotas and B. F. Schutz, Monthly Notices of the Royal Astronomical Society **255**, 119 (1992).
[5] K. D. Kokkotas and B. G. Schmidt, Living Reviews in Relativity **2**, 1 (1999).
[6] N. Andersson and K. D. Kokkotas, Monthly Notices of the Royal Astronomical Society **299**, 1059 (1998).
[7] H. Lau, P. Leung, and L. Lin, The Astrophysical Journal **714**, 1234 (2010).
[8] K. Yagi and N. Yunes, Physical Review D **88**, 023009 (2013).
[9] T. K. Chan, Y. H. Sham, P. T. Leung, and L. M. Lin, Physical Review D **90**, 124023 (2014).
[10] C. Chirenti, G. H. de Souza, and W. Kastaun, Physical Review D **91**, 044034 (2015).
[11] G. Lioutas, A. Bauswein, and N. Stergioulas, arXiv preprint arXiv:2102.12455 (2021).
[12] A. Reisenegger and P. Goldreich, Astrophysical Journal **395**, 240 (1992).
[13] W. Wei, M. Salinas, T. Klähn, P. Jaikumar, and M. Barry, The Astrophysical Journal **904**, 187 (2020).
[14] P. Jaikumar, A. Semposki, and M. Prakash, arXiv preprint arXiv:2101.06349 (2021).
[15] T. Zhao, C. Constantinou, P. Jaikumar, and M. Prakash, arXiv preprint arXiv:2202.01403 (2022).

[16] V. Dommes and M. Gusakov, Monthly Notices of the Royal Astronomical Society **455**, 2852 (2016).
[17] P. N. McDermott, H. Van Horn, and C. Hansen, The Astrophysical Journal **325**, 725 (1988).
[18] S. Y. Lau and K. Yagi, Physical Review D **103**, 063015 (2021).
[19] M. Rodríguez, I. F. Ranea-Sandoval, M. Mariani, M. Orsaria, G. Malfatti, and O. Guilera, Journal of Cosmology and Astroparticle Physics **2021** (02), 009.
[20] O. Benhar, V. Ferrari, and L. Gualtieri, Physical review d **70**, 124015 (2004).
[21] L. Rezzolla and K. Takami, Physical Review D **93**, 124051 (2016).
[22] V. Ferrari, G. Miniutti, and J. A. Pons, Monthly Notices of the Royal Astronomical Society **342**, 629 (2003).
[23] D. Radice, V. Morozova, A. Burrows, D. Vartanyan, and H. Nagakura, The Astrophysical Journal Letters **876**, L9 (2019).
[24] W. Li, R. Chornock, J. Leaman, A. V. Filippenko, D. Poznanski, X. Wang, M. Ganeshalingam, and F. Mannucci, Monthly Notices of the Royal Astronomical Society **412**, 1473 (2011).
[25] B. Margalit and B. D. Metzger, The Astrophysical Journal Letters **850**, L19 (2017).
[26] R. Oechslin and H.-T. Janka, Physical review letters **99**, 121102 (2007).
[27] M. Shibata, K. Taniguchi, and K. Uryū, Physical Review D **71**, 084021 (2005).
[28] A. Bauswein and H.-T. Janka, Physical review letters **108**, 011101 (2012).
[29] R. Abbott, T. Abbott, S. Abraham, F. Acernese, K. Ackley, A. Adams, C. Adams, R. Adhikari, V. Adya, C. Affeldt, *et al.*, The Astrophysical journal letters **913**, L7 (2021).
[30] D. Reitze, R. X. Adhikari, S. Ballmer, B. Barish, L. Barsotti, G. Billingsley, D. A. Brown, Y. Chen, D. Coyne, R. Eisenstein, *et al.*, arXiv preprint arXiv:1907.04833 (2019).
[31] N. Stergioulas, A. Bauswein, K. Zagkouris, and H.-T. Janka, Monthly Notices of the Royal Astronomical Society **418**, 427 (2011).
[32] H. H.-Y. Ng, P. C.-K. Cheong, L.-M. Lin, and T. G. F. Li, arXiv preprint arXiv:2012.08263 (2020).
[33] S. Ma, H. Yu, and Y. Chen, Physical Review D **101**, 123020 (2020).
[34] C. H. Wynn and L. Dong, Monthly Notices of the Royal Astronomical Society **308**, 153 (1999).
[35] J. Steinhoff, T. Hinderer, T. Dietrich, and F. Foucart, arXiv preprint arXiv:2103.06100 (2021).
[36] B. P. Abbott, R. Abbott, T. Abbott, F. Acernese, K. Ackley, C. Adams, T. Adams, P. Addesso, R. Adhikari, V. Adya, *et al.*, Physical Review Letters **119**, 161101 (2017).
[37] T. Hinderer, A. Taracchini, F. Foucart, A. Buonanno, J. Steinhoff, M. Duez, L. E. Kidder, H. P. Pfeiffer, M. A. Scheel, B. Szilagyi, K. Hotokezaka, K. Kyutoku, M. Shibata, and C. W. Carpenter, Physical review letters **116**, 181101 (2016).
[38] J. Steinhoff, T. Hinderer, A. Buonanno, and A. Taracchini, Physical Review D **94**, 104028 (2016).
[39] P. Schmidt and T. Hinderer, Physical Review D **100**, 021501 (2019), arXiv:1905.00818 [gr-qc].
[40] G. Pratten, P. Schmidt, and T. Hinderer, Nature communications **11**, 1 (2020).
[41] T. Sidery, A. Passamonti, and N. Andersson, Monthly Notices of the Royal Astronomical Society **405**, 1061 (2010).
[42] L. Keer and D. Jones, Monthly Notices of the Royal Astronomical Society **446**, 865 (2015).
[43] A. Basu, B. Shaw, D. Antonopoulou, M. J. Keith, A. G. Lyne, M. B. Mickaliger, B. W. Stappers, P. Weltevrede, and C. A. Jordan, Monthly Notices of the Royal Astronomical Society **510**, 4049 (2022).
[44] S. Konar and M. Arjunwadkar, arXiv preprint arXiv:1402.1594 (2014).
[45] N. Sartore, E. Ripamonti, A. Treves, and R. Turolla, Astronomy & Astrophysics **510**, A23 (2010).
[46] J. Fuentes, C. Espinoza, A. Reisenegger, B. Shaw, B. Stappers, and A. Lyne, Astronomy & Astrophysics **608**, A131 (2017).
[47] S. Detweiler and L. Lindblom, The Astrophysical Journal **292**, 12 (1985).
[48] Y. Kojima, The Astrophysical Journal **414**, 247 (1993).
[49] C. J. Krüger and K. D. Kokkotas, Physical Review D **102**, 064026 (2020).
[50] S. G. Rosofsky, R. Gold, C. Chirenti, E. A. Huerta, and M. C. Miller, Physical Review D **99**, 084024 (2019).
[51] S. Shashank, F. H. Nouri, and A. Gupta, arXiv preprint arXiv:2108.04643 (2021).
[52] C. Yip, M.-C. Chu, and P. Leung, The Astrophysical Journal **513**, 849 (1999).
[53] H. Sotani, N. Yasutake, T. Maruyama, and T. Tatsumi, Physical Review D **83**, 024014 (2011).
[54] C. V. Flores and G. Lugones, Classical and Quantum Gravity **31**, 155002 (2014).
[55] P. McDermott, H. M. Van Horn, and J. Scholl, The Astrophysical Journal **268**, 837 (1983).
[56] I. F. Ranea-Sandoval, O. M. Guilera, M. Mariani, and M. G. Orsaria, Journal of Cosmology and Astroparticle Physics **2018** (12), 031.
[57] D. Kumar, H. Mishra, and T. Malik, arXiv preprint arXiv:2110.00324 (2021).
[58] H. C. Das, A. Kumar, S. K. Biswal, and S. K. Patra, Physical Review D **104**, 123006 (2021).
[59] S. Yoshida and Y. Kojima, Monthly Notices of the Royal Astronomical Society **289**, 117 (1997).
[60] H. Sotani, K. Tominaga, and K.-i. Maeda, Physical Review D **65**, 024010 (2001).
[61] S. Chandrasekhar, VI. Ellipsoidal Figures of Equilibrium **1** (1960).
[62] T. G. Cowling, Monthly Notices of the Royal Astronomical Society **101**, 367 (1941).
[63] R. C. Tolman, Physical Review **55**, 364 (1939).
[64] H. A. Buchdahl, Physical Review **116**, 1027 (1959).
[65] G. Miniutti, J. Pons, E. Berti, L. Gualtieri, and V. Ferrari, Monthly Notices of the Royal Astronomical Society **338**, 389 (2003).
[66] C. Drischler, S. Han, J. M. Lattimer, M. Prakash, S. Reddy, and T. Zhao, Physical Review C **103**, 045808 (2021).
[67] J. S. Read, B. D. Lackey, B. J. Owen, and J. L. Friedman, Physical Review D **79**, 124032 (2009).
[68] B. Sharma, M. Centelles, X. Viñas, M. Baldo, and G. Burgio, Astronomy & Astrophysics **584**, A103 (2015).
[69] T. Zhao and J. M. Lattimer, Phys. Rev. D **98**, 063020 (2018).
[70] A. W. Steiner, J. M. Lattimer, and E. F. Brown, The European Physical Journal A **52**, 1 (2016).

[71] M. G. Alford, S. Han, and M. Prakash, Physical Review D **88**, 083013 (2013).

[72] S. De, D. Finstad, J. M. Lattimer, D. A. Brown, E. Berger, and C. M. Biwer, Physical review letters **121**, 091102 (2018).

[73] E. Benitez, J. Weller, V. Guedes, C. Chirenti, and M. C. Miller, Physical Review D **103**, 023007 (2021).

[74] L. Tsui and P. Leung, Monthly Notices of the Royal Astronomical Society **357**, 1029 (2005).

[75] G. Lioutas and N. Stergioulas, in *Journal of Physics: Conference Series*, Vol. 1667 (IOP Publishing, 2020) p. 012026.

[76] H. Sotani and B. Kumar, Physical Review D **104**, 123002 (2021).

[77] D.-H. Wen, B.-A. Li, H.-Y. Chen, and N.-B. Zhang, Physical Review C **99**, 045806 (2019).

[78] G. Montana, L. Tolos, M. Hanauske, and L. Rezzolla, Physical Review D **99**, 103009 (2019).

[79] F. J. Fattoyev, C. J. Horowitz, J. Piekarewicz, and B. Reed, Phys. Rev. C. **102**, 065805 (2020).

[80] L. S. Finn, Monthly Notices of the Royal Astronomical Society **227**, 265 (1987).

[81] L. D. Landau and E. M. Lifshitz, *Fluid Mechanics: Landau and Lifshitz: Course of Theoretical Physics, Volume 6*, Vol. 6 (Elsevier, 2013).

[82] M. G. Alford and S. P. Harris, Physical Review C **100**, 035803 (2019).

[83] L. Gualtieri, E. M. Kantor, M. E. Gusakov, and A. I. Chugunov, Phys. Rev. D **90**, 024010 (2014).

[84] M. Alford, A. Harutyunyan, and A. Sedrakian, Particles **3**, 500 (2020).

[85] P. Arras and N. N. Weinberg, Monthly Notices of the Royal Astronomical Society **486**, 1424 (2019).

[86] S. Chandrasekhar and V. Ferrari, Proceedings of the Royal Society of London. Series A: Mathematical and Physical Sciences **434**, 449 (1991).

[87] L. Tonetto and G. Lugones, Physical Review D **101**, 123029 (2020).

[88] E. Chabanat, P. Bonche, P. Haensel, J. Meyer, and R. Schaeffer, Nuclear Physics A **635**, 231 (1998).

[89] E. D. Fackerell, The Astrophysical Journal **166**, 197 (1971).

[90] N. Andersson, K. D. Kokkotas, and B. F. Schutz, Monthly Notices of the Royal Astronomical Society **274**, 1039 (1995).

[91] B. K. Pradhan, D. Chatterjee, M. Lanoye, and P. Jaikumar, arXiv preprint arXiv:2203.03141 (2022).

[92] W. Xu and D. Lai, Physical Review D **96**, 083005 (2017).

[93] M. Shibata, Physical Review Letters **94**, 201101 (2005).

[94] R. B. Wiringa, V. Fiks, and A. Fabrocini, Physical Review C **38**, 1010 (1988).